

Changes in the partial pressure of carbon dioxide were found to have little effect on this ratio.

It should be noted that the above dependence was determined in a fluidized bed. Available research suggests that for fixed beds, Equation (15) should be applied over the total bed length in order to obtain an integrated carbon-deposition rate (Dry, 1980). The dependence of carbon-deposition rate on partial pressures is different from the earlier observation that this rate was controlled merely by the  $H_2/CO$  ratio (Storch et al., 1951). The fact that increasing the reaction pressure decreases the rate of carbon formation is readily apparent from the above rate equation. Consequently, lower  $H_2/CO$  ratios of feed gases can be utilized when higher reaction pressures are used.

Dry et al. (1970) studied the Boudouard reaction, Equation (14a) over a fused-iron catalyst that had been converted to Hägg carbide. The goal of these studies was to obtain information about the role of promoters, and the influence of gas phase species on the rate of carbon deposition. As stated before, structural promoters (such as  $Al_2O_3$ ,  $CaO$  and  $SiO_2$ ) were found to merely increase the surface area of the catalyst. Chemical promoters that are strong bases, such as  $K_2O$ , were found to actually increase the intrinsic rate of the Boudouard reaction. Bonzel and Krebs (1981) reached a similar conclusion after studying carbon deposition under hydrogen and carbon monoxide on iron foils promoted with potassium.

In other research, Dry et al. (1970) perceived an increase in the rate of the Boudouard reaction on iron carbide in the presence of water

vapor, small amounts of hydrogen, aliphatic acids, alcohols, or ketones. The molecular hydrogen from these species was thought to enhance the rate of the Boudouard reaction. However, the increase in the rate of the Boudouard reaction was also found to be independent of the amount of the added gases.

#### 2.1.7.2 Mechanism and Nature of Carbon Formation

Carbon uptake and deposition on iron catalysts are characterized by two distinct rate regions. The first region is believed to be the diffusion-controlled formation of iron carbide; and the second is a slower rate of surface deposition of inactive carbon. Free carbon is typically observed after iron has been converted to carbide. This phenomenon has been observed in many studies. Typical ones are those by Pichler and Merkel (1949), Sancier, et al. (1979), Niemantsverdriet et al. (1980), Ott et al. (1980) and Krebs et al. (1981). Figure 2.9 illustrates the results of Sancier et al. (1979) over two calcined, promoted iron catalysts for F-T synthesis. The two distinct regions of weight gain can be seen in the figure.

The activity of the catalyst is affected by the carbon content of the catalyst. The activity generally increases as Hägg carbide is formed. It then goes through a maximum as carburization of the catalyst becomes complete and inactive carbon begins to form.

In Section 2.1.6.1, the competition model for carbon utilization was discussed with reference to Equations (13a) and (13c). In the model, surface reactions for the formation of bulk carbides, F-T chain intermediates, and inactive carbon are all in competition for surface

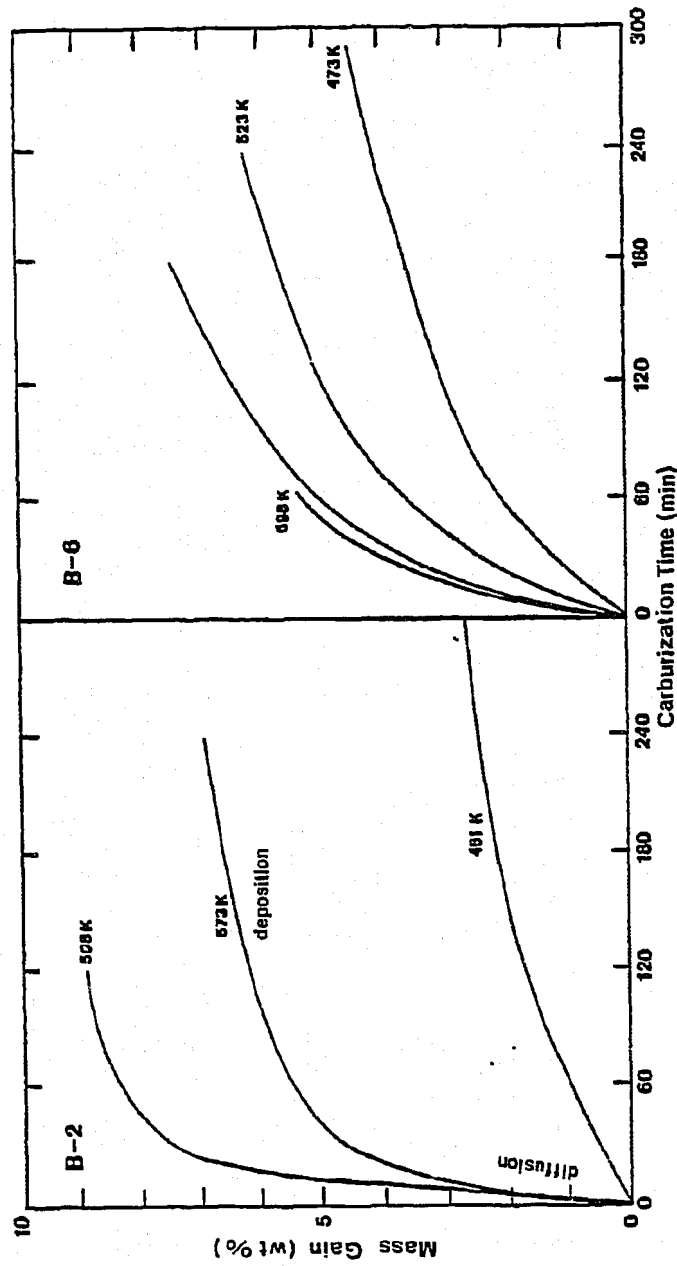


Figure 2.9. Two Distinct Regions of Mass Gain During Isothermal Carburization of Promoted Iron Catalysts B-2 and B-6 in H<sub>2</sub>/CO (3:1) at 101 kPa. (Sancier et al., 1979): "Diffusion" Indicating Diffusion-Controlled Formation of Iron Carbide and "Deposition" Indicating Surface Deposition of Inactive Carbon.

carbide species. Additional credence is lent to this model by Dry's (1981) finding that elemental carbon formation did not increase as the production of F-T synthesis products were increased. Therefore, inactive carbon is believed not to be produced as part of the product slate, but rather via another reaction scheme such as the competition model, Equations (13a) to (13c).

The exact mechanism for inactive carbon formation on iron catalysts is not known. It is thought to be similar to the mechanism on nickel catalysts. However, iron carbide most certainly plays a more important role in carbon formation on iron compared to that nickel carbides play in the nickel system (Trimm, 1982). A large body of studies has been reported on carbon formation in methanation (200-450°C) and steam reforming (600-900°C) over nickel catalysts. This information has been reviewed by Trimm (1977) and Bartholomew (1982). Carbon deposition on iron catalysts has not been pursued with the same zeal, most likely due to the complex mechanisms involved. The studies that have been performed generally focus on inactive carbon formation above 500°C (Kehrer and Leidheiser, 1954; Ruston et al., 1969; Renshaw et al., 1970; Boehm, 1973; Baker et al., 1982; Sacco et al., 1984).

The forms of carbon produced on iron catalysts have generally been deduced through analogy to carbon formation on nickel catalysts. Table 2.8 summarizes the possible forms of carbon species on metals, but primarily on nickel (Bartholomew, 1982). Adsorbed atomic carbon species,  $C_{\alpha}$ , are analogous to the surface carbidic species,  $C^*$ , suggested by Niemantsverdriet et al. (1981). In the case of iron

TABLE 2.8  
Forms and Reactivities of Carbon Species Formed by Decomposition  
of CO on Nickel (Bartholomew, 1982)

Structural type	Designation	Temperature (°C) formed	Peak temperature (°C) for reaction with H <sub>2</sub>
1. Adsorbed, atomic (dispersed, surface carbide)	C <sub>α</sub>	200-400	200
2. Polymeric, amorphous films or filaments	C <sub>R</sub>	250-500	400
3. Vermicular (polymeric, amorphous) a. filaments b. fibers c. whiskers	C <sub>V</sub>	300-1000	400-600
4. Nickel carbide (bulk)	C <sub>γ</sub>	150-250	275
5. Graphitic (crystalline) a. platelets b. films	C <sub>c</sub>	500 550	550-850

catalysts, it is believed that  $C_{\alpha}$  can convert to a less active, amorphous, form of carbon ( $C_{\beta}$ ) on the surface. This form of carbon has a low degree of organization and is associated with lower formation temperatures.  $C_{\beta}$  is thought to be a precursor to graphite formation. Amorphous carbon formation causes a decrease in catalytic synthesis activity through fouling via the encapsulation of metal crystallites. This occurs more readily on iron than on nickel catalysts (Cooper and Trimm, 1980). Amorphous carbon may also block pores decreasing the effective area for catalytic synthesis. Graphitic carbon typically forms as filaments of carbon and does not diminish catalytic activity. In fact, it may actually increase the activity of the catalyst by dispersing the iron in finely divided carbon.

It is believed that amorphous or poorly crystalline carbon is catalytically recrystallized by Hägg carbon or cementite. This carbon diffuses through the carbide phase, explaining why the rate of carbon deposition is diffusion-rate limited (Cooper and Trimm, 1980). Graphitic carbon then grows on a crystal face of the iron carbide by utilizing the carbon dissolved in the carbon lattice. This is shown in Figure 2.10 (Boehm, 1973). A particle or a crystal of iron may be contained in the head of this filament, as it grows. Finally, stress in the catalyst particle, caused by growing filaments and expanding regions of carbon, leads to particle disintegration. In an active environment such as a fluidized bed, filaments readily break off and catalyst particles crumble.

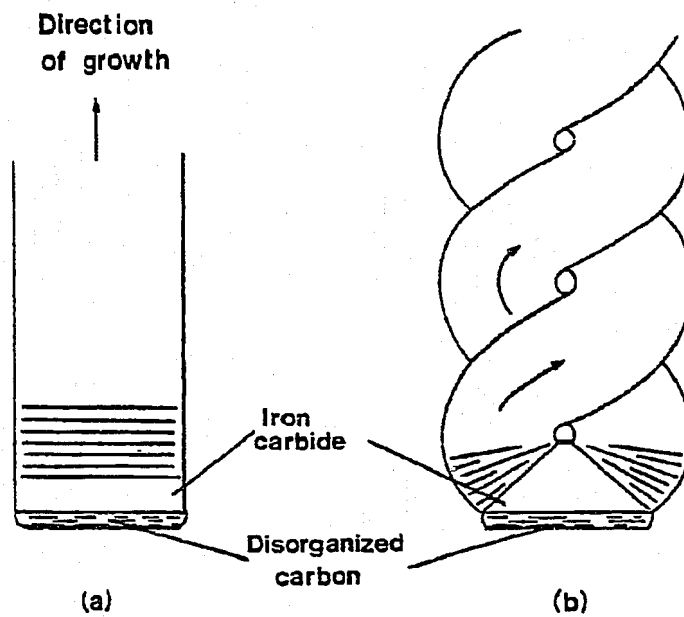


Figure 2.10. A Schematic Representation of the Growth Mechanism of Filamentary Carbon on Iron Carbide: (a) on a Rectangular Carbide Particle; and (b) on a Carbide Particle with Faces at Oblique Angles (Boehm, 1973).

Evidence of graphitic carbon formation on iron catalysts during F-T synthesis has been presented by several researchers. Reymond et al. (1980) using X-ray photoelectron spectroscopy (ESCA) showed graphite formed on a fused-iron catalyst at 250°C. Similarly, Agrawal et al. (1980) detected its formation of Fe/Al<sub>2</sub>O<sub>3</sub> at 237°C using Auger electron spectroscopy (AES). Krebs et al. (1981) found graphite to be formed at 297°C on both iron foil and reduced magnetite using X-ray photoelectron spectroscopy (XPS). Thus, graphitic deposits on iron surfaces have been shown to occur at relatively low temperatures under F-T synthesis conditions.

## 2.2 Unsteady-State Methods

Unsteady-state methods have generally been directed toward two objectives in the past. The first school of thought uses transient methods to discern the kinetics of a particular reaction, focusing on the elementary reaction mechanism. The second utilizes forced cycling of a reaction parameter (such as feed flow rate or reaction temperature) in order to attain improved selectivity and/or increased conversion from a given reaction. These two approaches invariably intertwine since both the reaction mechanism and operating parameters cannot be considered separately.

Reviews by Kobayashi and Kobayashi (1975) and Bennett (1976, 1982) generally focus on the use of the transient method as a tool to obtain fundamental kinetic information. Other reviews by Bailey (1973) and Boreskov and Matros (1983), approach the subject of unsteady-state



operation in a more applied sense, emphasizing the selectivity shifts and increased conversion.

### 2.2.1 Transient Method for Kinetic Studies

Transient methods for kinetic studies typically involve sending an input signal, such as a pulsed amount of reactant gases, into a reactor and then observing the time-dependent changes of certain reaction variables, such as reaction temperatures and species concentration. In order for the transient response to truly reflect the kinetics of the reaction being investigated, the reactor must be operated under conditions that are free of heat- and mass-transfer limitations. Transient experiments generally provide more information than steady-state experiments. Once the kinetic information has been obtained under transient conditions, it must be described by successive elementary steps (an elementary-step model). Similarly, the buildup of adsorbed intermediates on the catalyst during transients must be described by mass balances. If this model adequately describes the system under study, it can be used for reactor design calculations or control algorithms.

Forcing functions used in the transient method are generally generated using four-way chromatographic valves. Analytical methods for following the response typically involve the use of mass spectroscopy, and to a lesser extent, gas chromatography. Recently, in-situ surface techniques have been developed. The reactor itself is usually a differential reactor operating at atmospheric conditions and measurable conversions, resulting in simplified analysis. Use of

isotopic tracers allows transient kinetics to be studied without altering feed-gas concentrations. Complex surface interactions can be discerned by following the decay of labelled species on the catalyst surface after switching to an unlabelled feed.

A recent monograph edited by Bell and Hedegus (1982) includes many articles on catalysis under transient conditions; and two review papers by Bennett (1976, 1982) describe in some detail the basic theory and applications of transient methods in heterogeneous catalysis. Biloen (1983) also gives a brief summary of ideas to be considered when using transient kinetic methods.

Transient methods have been used in attempts to identify the reaction intermediates and rate-limiting steps in Fischer-Tropsch synthesis. For example, Matsumoto and Bennett (1978) and Raymond et al. (1980) applied the transient method to study the kinetics of the reaction of carbon monoxide with hydrogen to form methane. A promoted fused-iron catalyst was used in a tubular reactor at 250°C and atmospheric pressure. When a gas stream of the reaction mixture ( $H_2/CO = 9:1$ ) flowing over the catalyst was suddenly changed to pure hydrogen, large amounts of methane were formed. The surface of the catalyst was found to be covered mostly by a carbon intermediate, while the bulk of the catalyst was identified as Hägg carbide. The rate-determining step was found to be the hydrogenation of surface carbon. Similar studies on nickel methanation catalysts have identified two basic types of surface carbon on nickel catalysts (Wentrcek et al., 1976; McCarty and Wise, 1979).

Ino et al. (1981) found two kinds of carbon species using the transient method on a precipitated iron catalyst. A carbidic surface carbon was found to be highly reactive when exposed to hydrogen while amorphous free carbon was less reactive. Kieffer and Van Der Baan (1982) suggested that the rate of propagation of hydrocarbon chains could not be the rate-determining step of F-T synthesis. This conclusion was reached from transient experiments in a microreactor packed with precipitated iron-zinc catalysts at 277°C and 2.5 atm. More recently, Bennett and coworkers (Bianchi et al., 1983) used the transient method in conjunction with in-situ Mössbauer effect spectroscopy to study surface and bulk changes in an Fe/Al<sub>2</sub>O<sub>3</sub> catalyst. These surface species were discovered: (1) CH<sub>x</sub>, a reactive species; (2) CH<sub>y</sub>, a less reactive species; and (3) an inert "graphite-like" species. Bennett and coworkers (Underwood and Bennett, 1984; Suib et al., 1984) have also examined the reaction of hydrogen and carbon monoxide over nickel-alumina catalysts, as well as F-T synthesis over iron-containing zeolites using the transient method.

The transient method has been used to study methanation and F-T synthesis reactions over alumina-supported ruthenium catalysts as well. Dautzenberg et al. (1977) used 3% Ru on  $\gamma$ -Al<sub>2</sub>O<sub>3</sub> in a fixed-bed reactor at 210°C and 10 bar. A H<sub>2</sub>/CO mixture of 1:1 ratio was passed over the catalyst for several minutes followed by pure hydrogen. In addition, the bed temperature was cycled to 350°C and then rapidly cooled to 210°C. The purpose of this transient study was to determine the rate constants of the propagation reaction for the production of

hydrocarbon chains. Cant and Bell (1982) used transient response tracing in conjunction with in-situ infrared spectroscopy to determine the elementary steps of CO hydrogenation over ruthenium catalysts.

### 2.2.2 Improved Conversion and Selectivity

Based on theoretical and computational studies, Bailey and Horn (1967, 1971) and Douglas and Rippon (1966, 1967) have suggested that selectivity improvements can be made by cycling the reactor feed-concentration. Silverston, Hudgins and coworkers (Unni, et al., 1973; Abdul-Kareem et al., 1980; Jain et al., 1982a, 1982b, 1982c, 1983a, 1983b) have experimentally shown that the forced cycling of feed composition can significantly increase the catalyst activity.

In a review paper, Bailey (1973) describes periodic operation in terms of two characteristic terms: (1) the period or cycle time,  $\tau$ ; and (2) the characteristic response time of the system,  $\tau_c$ . A quasi-steady-state system (QSS) results from the imposition of periodic behavior on a system, where the cycle time is much greater than the response time of the system ( $\tau \gg \tau_c$ ). More product can be obtained through QSS operation using an equivalent amount of reactants as in steady-state operation, but by cyclic feeding. The most important concept for QSS systems is that their output can be obtained by "mixing the outputs of several parallel processes operated at different steady states." In the latter operational mode, it seems to be more economical to run several parallel reactors and mix the outputs than to operate one system cyclically.

A second type of operation is termed relaxed steady-state. Here, the response time of the system is much slower than the cycle time of the forcing function ( $\tau \ll \tau_c$ ). The system is unable to follow the rapid cycling and produces a time-invariant state, which may be called a relaxed steady-state.

Intermediate periodic operation is the final condition mentioned by Bailey (1973). In this case, the cycle time and the system response time are generally of the same order of magnitude.

Whether or not forced unsteady-state operation has an effect on a heterogeneous system depends on how the changing reaction medium affects the catalyst and on the dynamics of the reactor system itself (Boreskov and Matros, 1983). By manipulating reactor inlet parameters such as composition, temperature, pressure and space velocity in a periodic fashion, unsteady-state conditions can be maintained. The constantly changing reaction medium can influence the catalyst in two ways. The concentration of surface intermediates can change from what they were in steady-state. Alternately, the state of the catalyst surface itself can differ from when it was under the steady-state fluid composition. As discussed in previous sections, F-T synthesis catalysts in particular are dynamic parts of the reaction system. The bulk and surface compositions of F-T synthesis catalysts depend both on temperature and feed composition.

Hudgins, Silverston and coworkers (Jain et al., 1983) have introduced certain nomenclature that facilitates understanding in the study of periodic operation. Figure 2.11 is a plot of an optimization

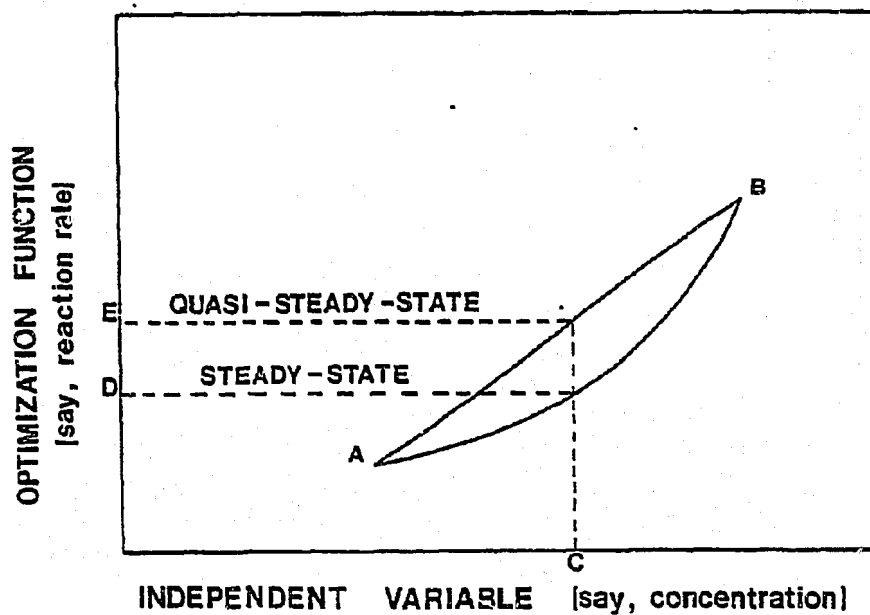


Figure 2.11. The Relationship Between the Steady-State and Quasi-Steady-State Kinetic Systems (Jain et al., 1983b).

function (such as reaction rate) versus an independent operating variable (such as feed concentration). Curve AB is the experimental reaction rate determined at various reactant concentrations for steady-state operation. For a given reactant concentration labelled by C in the figure, a reaction rate, labelled by D, will be observed at the steady state. Point E in the figure represents the reaction rate at the quasi-steady state. Recalling the description of QSS above, point E would be obtained by appropriately weighting the reactant feeds and mixing their outputs. Periodic operation would be obtained if the feed composition to a reactor is cycled between two concentrations, labelled A and B in the figure. This would result in a mean concentration, C.

If the above periodic operation is achieved by using a square-wave input signal, several more terms are defined. Figure 2.12 illustrates the terms used in cycling operations. The period,  $\tau$ , is the time necessary for one full cycle. The cycle split,  $s$ , is the ratio of the time for the first partial cycle to the period ( $\tau$ ). The line segment AB in Figure 2.11 thus represents a series of quasi-steady-state reaction rates. These are the maximum reaction rates that can be obtained by mixing the outputs of parallel steady-state reactors. Therefore, any improvement in the time-average reaction rate would correspond to a point above the quasi-steady-state line segment AB. This point would accordingly be beyond the range of steady-state rates under the same time-averaged values of pressure, temperature and composition. If the steady-state curve were concave downward instead, the quasi-steady-state line would lie below the curve.

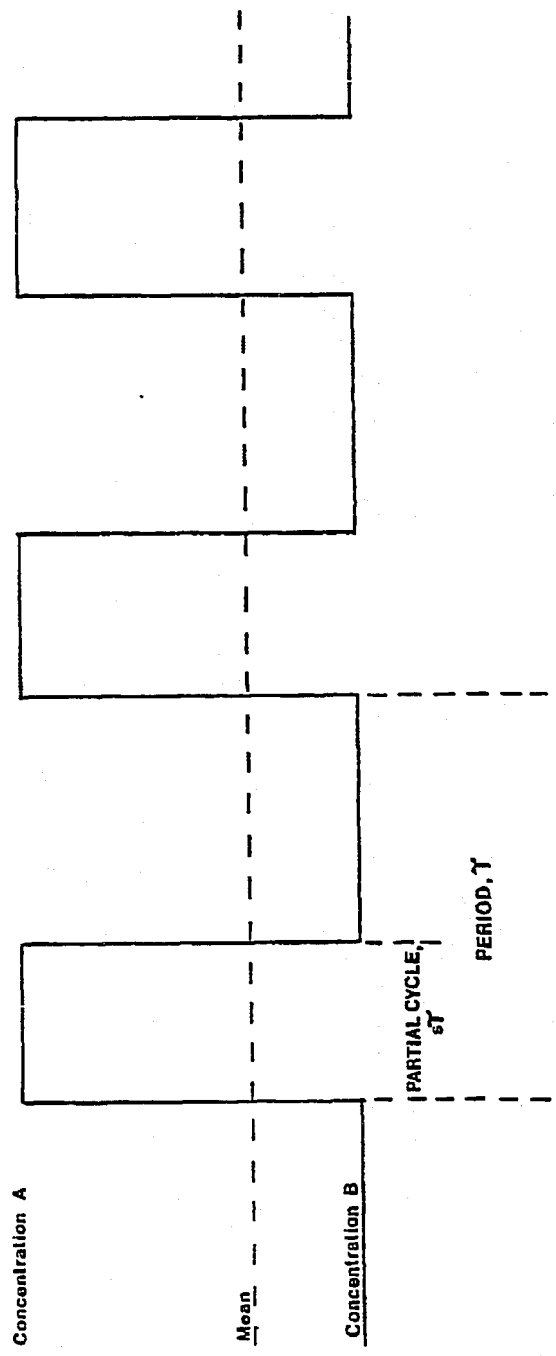


Figure 2.12. An Illustration of Terms Used in Cycling Operations (Jain et al., 1983b).



Using the above unsteady-state operational concepts and definitions, a systematic study of carbon-deposition rate as a function of ratio of hydrogen to carbon monoxide in the feed in a cycled-feed system could be undertaken. This was an objective of the present study.

Table 2.9, as adopted from Boreskov and Matros (1983) with several additions, lists processes where improvements in product selectivity and reactant conversion have been attained through unsteady-state operations. One representative example of these processes is ammonia synthesis on fused-iron catalysts as studied by Jain et al. (1982a, 1982c, 1983b). Cycling between a nitrogen-rich (hydrogen-poor) and a nitrogen-poor (hydrogen-rich) gas using periods of one to sixty minutes, it was found that the time-averaged reaction rate could be improved between 30 to 50 percent. Conditions of the synthesis were 23.8 atm and 360-400°C. These researchers speculate that nitrogen is dissolved in the bulk phase of the iron catalyst during the nitrogen-rich concentration portion of the cycle. The nitrogen diffuses back to the catalyst surface when the gas-phase concentration of nitrogen is low.

Only two experimental studies and one theoretical paper have examined possible selectivity improvements in Fischer-Tropsch synthesis. These studies were carried out in part to attempt to shift the standard "polymerization distribution law" or "Flory" distribution towards liquid products and away from high-molecular-weight species. Dautzenberg et al. (1977), cited previously, claimed selectivity improvements over a Ru/Al<sub>2</sub>O<sub>3</sub> catalyst. A synthesis gas of a H<sub>2</sub>/CO ratio of 1:1 was passed over the catalyst for 4 to 12 minutes, followed by pure hydrogen at an elevated temperature. It was shown that as the

TABLE 2.9  
 Examples of Processes Performed Under Forced Unsteady-State Conditions  
 (Adapted from Borekov and Matros, 1983)

Process	Forcing Variable	Effect	Reference
1. Synthesis of ammonia on iron	Initial mixture composition	Increase in rate of conversion	Jain et al. (1982c, 1983b)
2. Oxidation of CO over V <sub>2</sub> O <sub>5</sub>	Initial mixture composition	Increase in rate of conversion	Abdul-Kareem et al. (1980)
3. Oxidation of CO over platinum	Initial mixture composition	Increase in rate of conversion	Cutlip (1979)
4. Oxidation of sulfur anhydride on vanadium catalyst	Initial mixture composition	Increase in rate of conversion	Unni et al. (1973) Briggs et al. (1977)
5. Polymerization of olefins on Ziegler-Natta catalysts	Hydrogen concentration	Change in the distribution of molecular weights	Claybaugh et al. (1969)
6. Polymerization of styrene	Concentration of styrene and initiator	Increase in yield	Crone and Renken (1979)
7. Production of ethyl acetate in a stationary catalyst bed	Concentration of acetic acid	Decrease of catalyst deactivation	Leupold and Renken (1977)
8. Ethylene hydrogenation on platinum-aluminum catalyst	Space velocity of the initial mixture	Increase of productivity	Renken et al. (1975) Baiker and Richarz (1976) Heirick et al. (1974)
9. Ethylene oxidation on supported silver catalyst	Initial mixture composition	Increase of selectivity	Renken et al. (1976)
10. Chlorination of n-decane in a two-phase adiabatic reactor	Concentration of n-decane	Change in selectivity	Yang et al. (1974)

TABLE 2.9 (continued)

Process	Forcing Variable	Effect	Reference
11. Ethanol dehydrogenation in a catalyst bed	Temperature of the cooling agent	Increase rate of conversion	Denis and Kabel (1970a,b)
12. Liquid-phase hydrogenation of <i>n</i> -methyl styrene on palladium catalyst	Space velocity of the initial mixture	Increase of productivity	Bisks and Smith (1963)
13. Oxidation of butane, cyclohexane on platinum nets	Initial mixture composition	Change in selectivity	Handrey and Ilenken (1977)
14. Oxidation of SO <sub>2</sub> on vanadium catalyst	Switching of the direction of the reaction mixture flow in the catalyst bed	Reduction of capital investments; possibly to process gases with variable and low initial concentration; increase of conversion	Boreskov and Matros (1983)
15. Catalytic detoxication of various industrial gases from CO and organic substances	Switching of the direction of the reaction mixture flow in the catalyst bed	Reduction of capital investments, possibly to process gases with variable and low initial concentration; increase of conversion	Boreskov et al. (1981a, 1982a)
16. Synthesis of ammonia on iron catalyst	Switching of the direction of the reaction mixture flow in the catalyst bed	Reduction of capital investments, possibly to process gases with variable and low initial concentration; increase of conversion	Boreskov et al. (1981b)
17. Oxidation of sulfur anhydride on vanadium catalyst	Temperature of inlet mixture	Increase of conversion	Boreskov et al. (1982a,b)

chain length increased, deviations from the polymerization distribution law became greater. This claim was made by simply comparing unsteady-state experimental results to the theoretical product distribution predicted by the polymerization distribution law. No steady-state experimental results were presented. Madon (1979) later pointed out that the polymerization distribution law did not apply to data obtained over alumina-supported ruthenium catalysts. Madon et al. (1977) have shown steady-state product distributions that are similar to those of Dautzenberg et al. (1977) obtained under cyclical conditions on Ru/Al<sub>2</sub>O<sub>3</sub>.

Feimer et al. (1981, 1982b, 1984) studied the effect of forced cycling of hydrogen and carbon monoxide concentration in the feed gas over a precipitated, copper-potassium-promoted iron catalyst in a fixed-bed reactor at 246°C and 3.8 atm. Differential conversions were measured using pulsed amounts of hydrogen-rich and hydrogen-poor mixtures of H<sub>2</sub> and CO for different time periods varying from one to thirty minutes. Steady-state and step-change measurements were also undertaken to supplement the cycling studies. The step-change experiments suggest that altering the H<sub>2</sub>/CO ratio in the feed gas changes the relative amounts of hydrogen and carbon monoxide adsorbed on the surface of the iron catalyst. Under rapid cycling with one pulse containing pure hydrogen, methane was produced at a rate 80% higher than the corresponding reaction under steady-state conditions. This was taken as evidence that methane was produced via hydrogenation of a surface carbide as well as through the standard chain-building route.

The results also indicated that a decrease in the time period between hydrogen-rich and hydrogen-poor pulses increased the time-averaged production rates of higher hydrocarbons. However, these production rates were smaller than those observed under steady-state conditions. These investigators thus suggested that under their experimental conditions, no significant improvement in rate or selectivity to liquid hydrocarbons could be achieved. It follows that their results obey the polymerization distribution law with the exception of methane.

As discussed earlier, Peacock-Lopéz and Lindenberg (1984) showed that the use of transient operating conditions may, theoretically, significantly alter the F-T product distribution. This model predicts, in one instance, that a majority of products being produced would be C<sub>5</sub> to C<sub>20</sub>, or liquid products. For a steady-state reaction with the same probability of chain growth ( $\alpha$ ), the polymerization distribution law suggests that the majority of products will contain 20 or more carbon units. One important conclusion of this study was that deviations from the polymerization distribution law were more pronounced as the probability of chain growth approached unity (i.e.,  $\alpha > 0.9$ ).

Note that the probability of chain growth can be altered in three ways: (1) by selecting different types of catalysts; (2) by adjusting catalyst promoter content; and (3) by altering the synthesis conditions. Catalyst selection has the most pronounced effect on the probability of chain growth. Jacobs and Van Wouwe (1982) describe typical bounds on this parameter for F-T synthesis catalysts:

Fe  $\alpha = 0.50-0.70$

Co  $\alpha = 0.70-0.80$

Ru  $\alpha = 0.85-0.95$

If the results by Feimer et al. (1981, 1982b, 1984) are examined in light of Peacock-Lopéz and Lindenberg's (1984) prediction, it is understandable why no deviation from the polymerization distribution law model was observed. Feimer and coworkers obtained a probability of chain growth of approximately 0.67 on their precipitated and promoted iron catalyst. This observed probability was well below the values necessary to show deviations.

### 2.3 Vibrofluidized Beds

A vibrofluidized bed is typically created by imparting vertical sinusoidal vibrations to a vessel containing a granular solid. In a conventional fluidized bed, particles are bouyed up from beneath throught the action of gas impinging on the particle. A vibrofluidized bed, however, typically does not have a fluidizing gas flowing through it from below.

Recently, a distinction has been made between systems with and without a forced fluidizing gas flow from beneath. Systems without a forced gas flow from beneath, yet possessing vibrational accelerations  $A\omega^2/g > 1$ , are termed "vibrated beds" ( $A$  = vibrational amplitude in length;  $\omega$  = angular frequency in radians per second;  $g$  = acceleration due to gravity). All beds with  $A\omega^2/g > 1$  and gas velocities less than the minimum fluidization velocity ( $U_{mf}$ ) for gas-fluidization are termed "vibrofluidized beds." Finally, all beds with gas velocities greater

than  $U_{mf}$  for gas fluidization that are also being vibrated at any frequency are called "vibrated fluid beds." These terms were defined in a recent review of the theory and applications of vibrated beds and vibrated fluid beds (Pakowski et al., 1984). A detailed review of vibrofluidized beds and their applications has been presented by Hirt (1984).

Vibrofluidized beds possess characteristics which make them uniquely different from conventional gas-fluidized beds. Vibrofluidized beds can operate at very low gas flow rates, consequently extending the range of fluidization. A uniform gas distribution can be readily achieved in a vibrofluidized bed, eliminating channelling or gas-bubble formation as observed in gas-fluidized beds. The solid, nevertheless, is intensely mixed by the vibration. This vigorous mixing promotes both heat and mass transfer between the particles and the gas, as well as, heat transfer to the walls. Excellent heat transfer results in a virtually isothermal bed. These characteristics lead to an uninterrupted phase of gas and solid of uniform bed height with little backmixing of gas under most conditions (Chlenov and Mikhailov, 1964, 1965; Baird, 1966; Bratu and Jinescu, 1971).

Bachman (1940) was probably the first to describe and attempt to model the dynamic behavior of particles inside a vibrated, vertical cylinder. Kroll (1955) also examined solid circulation in a vibrated vessel. Enhanced heat transfer coefficients in vibrated beds were found by Bratsnajder et al. (1963). About the same time, Chlenov and Mikhailov (1964, 1965) coined the term "vibro-fluidization." These two

researchers were also the first to suggest practical uses for vibrofluidized beds. They advocated its use for drying of the free-flowing material, roasting of granules and reduction of metals. They noted that because of their unique characteristics, vibrofluidized beds would be particularly well suited for exothermic reactions.

In the first laboratory application of vibrofluidized beds to catalytic reactions, Shchel'tsyn et al. (1968) used a vibrofluidized bed to screen catalysts and determine the kinetics of the gas-phase vinylation of  $\alpha$ -pyrrolidone. In this study, 35 to 50 ml of 0.25-1 mm diameter catalyst particles were charged to the reaction vessel. The vibrofluidized bed used did not have a permeable base plate, but rather  $\alpha$ -pyrrolidone vapor was introduced to the base of the bed via a trumpet-shaped dip tube. The reaction was run at 260-320°C, 1 atm with a  $\alpha$ -pyrrolidone vapor space-velocity of 250 hr<sup>-1</sup>. The vibration frequency of the reaction vessel was set at 100 cycles per second, which resulted in ideal solid mixing with no diffusional reaction limitation.

No other references to the use of vibrofluidized beds as catalytic reactors could be found in the literature. Several references to vibrated fluid-beds for gas-solid and gas-phase catalytic reactors have been found. Wronski et al. (1976) procured a patent in Poland for desublimation of phthalic anhydride vapors in a vibrated fluidized bed. The vapors were condensed in a bed of particles vibrating at 15 Hertz (or cycles per second) with an amplitude of 15 mm. The effect of grid-plate vibration rate on the mass transfer coefficient was the subject of experiments by Reusov et al. (1980). Mass transfer between the fluid and solid was found to increase significantly with increasing vibration rate



and fluid flow rate, and with decreasing bed porosity. Also in 1980, Alekseeva et al. examined the catalytic oxidation of HCl to Cl<sub>2</sub> over CuCl<sub>2</sub> and KCl. A 25-ml vibrated fluidized-bed reactor was used for studies at temperatures ranging from 387-427°C. More recently, the kinetics of the catalytic pyrolysis of ethane were investigated in a vibrated fluidized bed. Indium-oxide (In<sub>2</sub>O<sub>3</sub>) catalyst was vibrated at a frequency of 20-25 Hz and an amplitude of 2-3 mm in the presence of ethane diluted with oxygen. The reaction conditions were 650-800°C and presumably 1-atm total pressure.

Several observations can be made from the above examination of reaction studies in vibrofluidized and vibrated fluid beds. First, a vast majority of work on this subject originates from the Soviet Union and Eastern Europe and, therefore, has been written in languages other than English. This results in a very slow transfer of concepts to English-speaking researchers. Secondly, most if not all of these studies have been performed at low pressures. Vibrofluidized beds can, of course, operate under high pressures as well as high temperatures. In this work, a vibrofluidized-bed microreactor has been developed for F-T synthesis studies at approximately 2,200 kPa (about 22 atm) and nearly 400°C.

CHAPTER 3  
EXPERIMENTAL APPROACH

3.1 An Overview

As discussed in Section 2.2, unsteady-state operation of chemical reactors has been shown to improve the conversion and/or selectivity of several reactions. The ultimate goal of the research undertaken at Virginia Tech is to determine if a reduction in carbon deposition on a promoted fused-iron catalyst can be achieved through rapid forced concentration-cycling of microreactor feed gases. It is hoped that through cycling of a feed gas of a low H<sub>2</sub>/CO ratio (< 1:1) followed by a hydrogen-rich feed gas, active surface carbon will be utilized before it can degrade into an inactive form. It is also hoped that that cycling of feed gases in this manner would simulate the catalyst residence time in the heat-tray reactor described previously in Chapter 1.

The experimental studies presented in this dissertation have been broken down into three phases:

1. Steady-State Fischer-Tropsch Synthesis in a Vibrofluidized-Bed Microreactor System.
2. Gas Mixing and Catalyst Vibrofluidization Studies in a Cold-Flow Vibrofluidized-Bed Microreactor Model.
3. Design and Construction of a Vibrofluidized-Bed Microreactor System for Unsteady-State Fischer-Tropsch Synthesis.

The first phase involved obtaining information on carbon deposition under steady-state synthesis conditions as well as determining operating conditions. The second phase required characterization of a newly developed unsteady-state microreactor system by using a cold-flow model.

The final phase utilized the results obtained from the cold-flow microreactor model to design a high-pressure, high-temperature system for unsteady-state Fischer-Tropsch synthesis. Using the unsteady-state vibrofluidized-bed microreactor system developed here, investigations of the effect of feed cycling on carbon-deposition rate during F-T synthesis will be performed in the near future.

### 3.2. Steady-State and Unsteady-State Carbon Deposition Studies

Researchers at the University of Waterloo have developed a nomenclature for the study of forced concentration feed cycling (Jain et al., 1983b). This system has been explained in Section 2.3.2. Implementation of their concepts results in a plot of the optimization function versus an independent variable as shown in Figure 2.11. By plotting unsteady-state experimental results on such a plot, any improvement over steady-state operation can be seen.

In the present study, the optimization function is the carbon-deposition rate, while the mole fraction of hydrogen in the feed can be taken as an independent variable. As an example, Dry's equation for carbon deposition rate, Equation (15) in Section 2.1.7.1, can be used to construct a steady-state carbon-deposition rate curve. For this example, the relative partial pressures of  $H_2$  and  $CO$  are assumed to be constant throughout the reactor. If a feed gas of a  $H_2/CO$  ratio of 0.11:1 (point A in Figure 3.1) were fed for 3/4 of a cycle and pure hydrogen (point B in Figure 3.1) were fed for the remainder of the cycle at the same flow rate, the mean composition of the feed gas would have a  $H_2/CO$  ratio of 0.44:1 (point C in Figure 3.1). The quasi-steady-state carbon-deposition

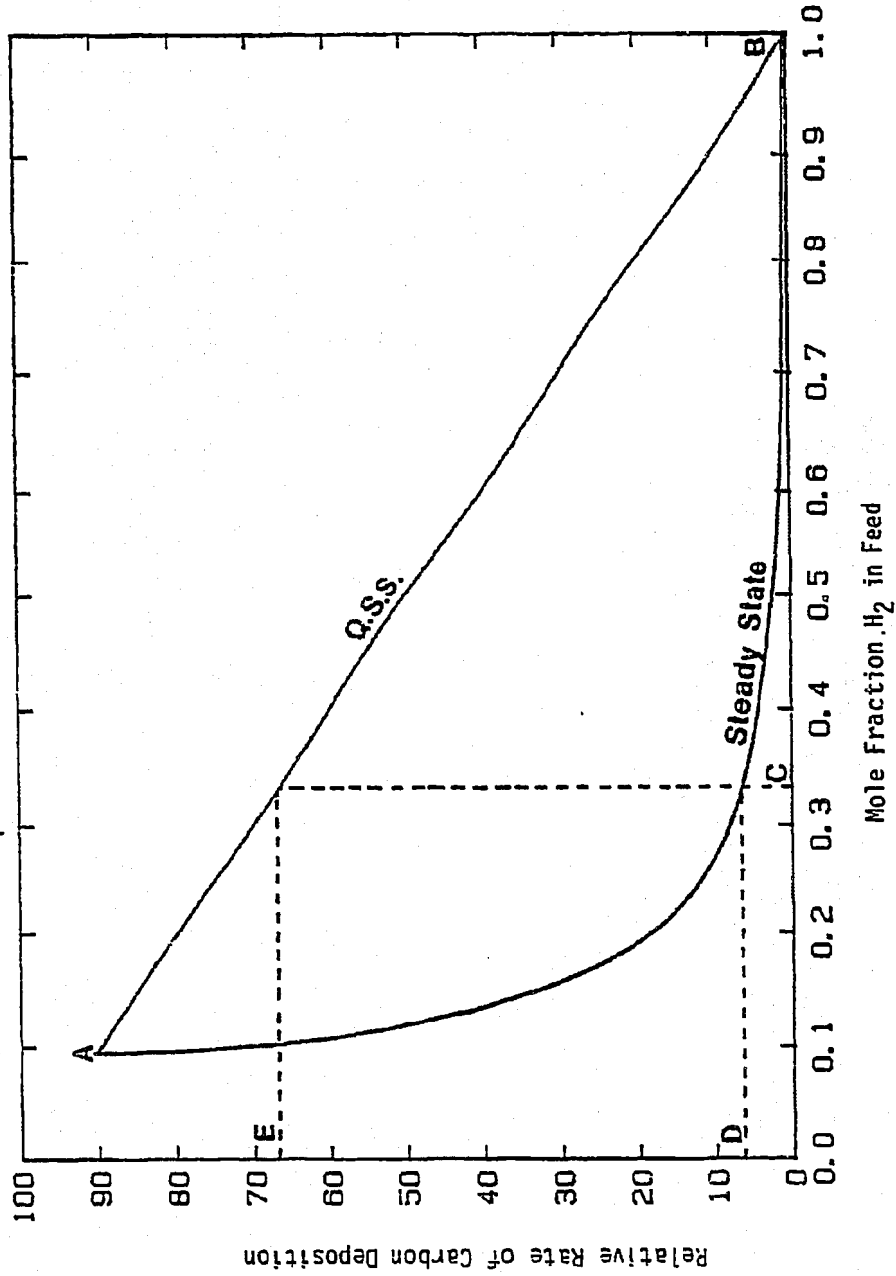


Figure 3.1. Hypothetical Quasi-Steady-State (Q.S.S.) and Steady-State Carbon-Deposition Rate Curves for Carbon Deposition as a Function of H<sub>2</sub> Mole Fraction in Feed.

rate would correspond to that given by point E in Figure 3.1. Point D in the figure is the rate that would be obtained through the steady-state reaction of the mean-composition gas. Any improvement, therefore, would be expressed by a reduction of carbon-deposition rate below the steady-state rate given by point D.

In reality, carbon-deposition rate is a function of the partial pressures of hydrogen and carbon monoxide in the reactor. These partial pressures, in turn, depend on the feed-gas composition and the reaction conditions. The partial pressures of  $H_2$  and  $CO$  vary through the catalyst bed and are affected by the extent of reaction and by the water-gas shift reaction. A proper study of the effect of forced feed-concentration cycling on the carbon-deposition rate during F-T synthesis would involve:

1. The determination of steady-state rates of carbon deposition as a function of feed partial-pressures of hydrogen and carbon monoxide.
2. The determination of unsteady-state rates of carbon deposition as a function of cycle split. Cycle split is defined as the duration of the cycle during which one concentration feed gas is being feed relative to the total cycle period. A feed with the same partial pressures of hydrogen and carbon monoxide as was chosen for the steady-state studies should be used.
3. The comparison of results from both steady-state and unsteady-state experiments.

## CHAPTER 4

### STEADY-STATE FISCHER-TROPSCH SYNTHESIS IN A VIBROFLUIDIZED-BED REACTOR SYSTEM

#### 4.1 Experimental Apparatus and Procedures

##### 4.1.1. Experimental Apparatus

##### 4.1.1.1 Microreactor System

Fischer-Tropsch experiments were performed in a specially-designed vibrofluidized-bed microreactor system operated isothermally in the range of 360 to 400°C. All experiments were undertaken at a total system pressure of 2,220 kPa (320 psia or 22 atm).

All steady-state experiments were performed in a reactor system that also functioned as a preliminary design for the unsteady-state experimental apparatus.

Figure 4.1 is a schematic of this steady-state vibrofluidized-bed reactor system. Premixed feed gases, either a H<sub>2</sub>:CO:Ar mixture or pure hydrogen, enter the system through stainless-steel high-pressure regulators (Airco model 49). The feed gas then passes through an activated-carbon filter used to remove impurities followed by a 15-micron filter which protects downstream solenoid and needle valves. The gas is stored upstream of solenoid valves 1-4 at 4,811 kPa in 1000-ml 304-stainless-steel sample cylinders. Two-way, normally-closed, high-pressure solenoid valves are used to select gas flow to the reactor. These solenoid valves (1-4), and also downstream solenoid valve 5, are stainless-steel valves (Circle Control model SV10) with Nylatron seats. Low-flow stainless-steel needle valves (Nupro series SG and SGD) are

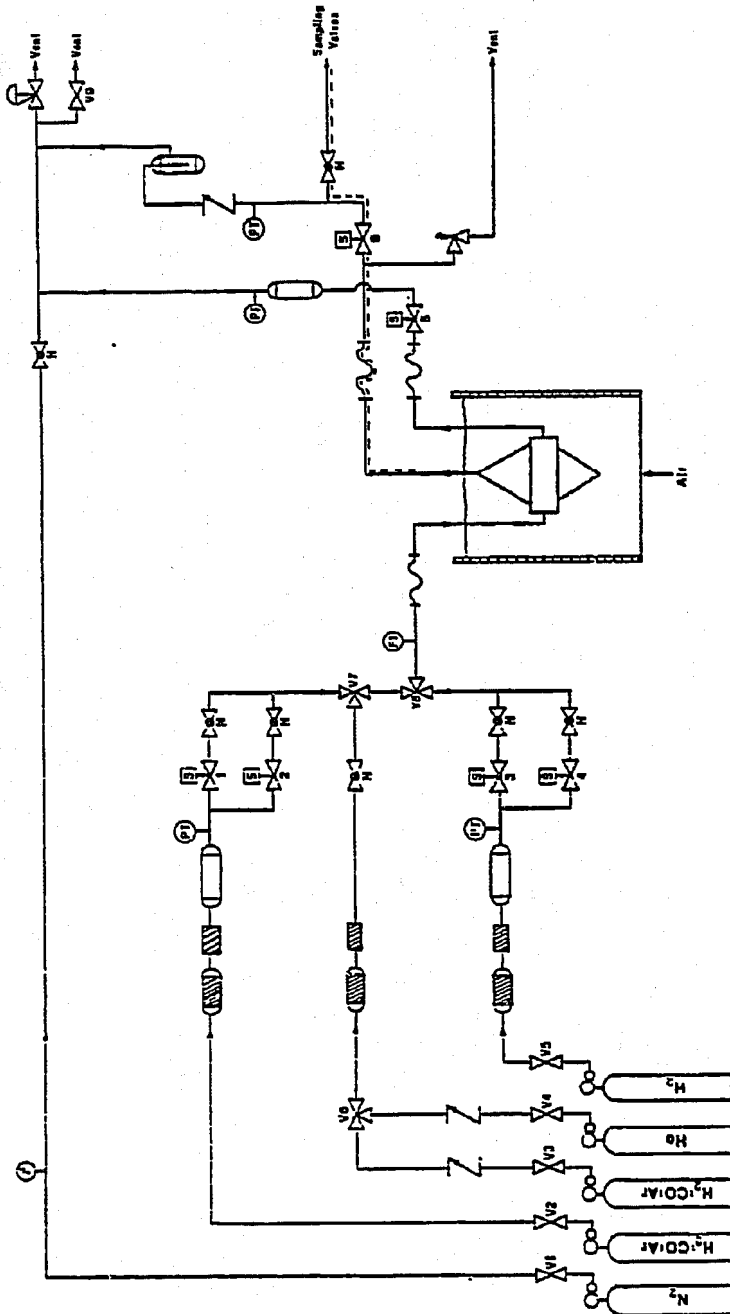


Figure 4.1a. A Schematic Diagram of the Steady-State Vibro-fluidized-Bed Microreactor System.













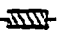


	Two - way Valve	O <sub>1</sub>	Valve Oven
	Needle Valve	O <sub>2</sub>	G.C. Oven
	Solenoid Valve	P	F-T Products
	Three-way Valve	V <sub>1</sub>	6-Port Sample Valve
	Check Valve	V <sub>2</sub>	10 - Port Sample Valve
	Pressure Relief Valve	S <sub>1</sub>	0.03 ml Sample Loop
	Gas Reservoir	S <sub>2</sub>	0.2 ml Sample Loop
	Flow Transducer	C <sub>1</sub>	Capillary Column
	Pressure Transducer	C <sub>2</sub>	Packed Column
		INT.	Reporting Integrator
	Microreactor	FID	Flame Ionization Detector
	Flexible S.S. Hose	TCD	Thermal Conductivity Detector
	Carbon Filter		Filter
	Liquid Trap		Pressure Gauge

Figure 4.1b. Equipment Symbols Used in Figures of Experimental Systems.



used in conjunction with a Thermal Mass Flowmeter (Brooks model 5810) to manually set feed-gas flow rates.

A critical pressure drop is maintained across the needle valves, making the flow rate through these valves independent of downstream pressure. Creating a critical pressure drop involves setting the upstream pressure at a sufficiently high pressure, thereby causing gas flows through the needle valves to be at the sonic velocity. A three-way valve in the synthesis gas line after solenoid valve 2 allows for switching to helium feed for system purging or to a synthesis gas of a higher  $H_2/CO$  ratio for precarburation of the catalyst.

The reactor itself is suspended down into a constant-temperature fluidized bath (Techne SBL-2D) where its temperature is controlled to  $\pm 1^\circ C$  by a controller (Techne model TC4). Flexible stainless-steel hoses connect the fixed feed- and exit-gas lines to the vibrating microreactor. The exit line from the right-hand side of the microreactor is used only for purging gases from the reactor-feed line. This purge line was originally designed for use during unsteady-state F-T synthesis experiments. Therefore, solenoid valve 5 is kept closed during steady-state operations.

The vertical line exiting the top of the microreactor is the product exit line. Synthesis gas or reducing hydrogen enters the reactor from the left-hand feed-gas line, passes up through the vibrofluidized catalyst bed where it is converted and exits through the heated product exit line. This line is traced with heating tape and is held at  $200^\circ C$ .

Solenoid valve 6 is a high-temperature, high-pressure, normally-closed valve. It is a series-1000 stainless-steel unit with a Teflon seat manufactured by Atkomatic Solenoid Valves. This valve is held open during catalyst reduction and synthesis. A double-needle valve (Nupro Model SGD) allows for a small amount of product gas to be drawn off continuously through 1/16-inch O.D. stainless-steel tubing for sample analysis by gas chromatography.

System pressure is maintained at 2,220 kPa through the use of a back-pressure regulator (BPR) manufactured by Circle Seal Controls (model number BPR-8A). The back-pressure regulator maintains the system pressure within  $\pm 35$  kPa, when a nitrogen ballast gas flow is used. The flow rate of product gases through the back-pressure regulator is normally too small to keep the BPR from "searching." Therefore, a larger, constant flow of nitrogen is used to supplement the product-gas flow through the BPR.

A check valve and a liquid trap lie between the product exit line and the nitrogen ballast line. The system pressure is monitored by two strain-gage absolute-pressure transducers (Schaevitz type P720). By using these transducers in connection with 3-way valves, pressure can be read in more than one position if care is exercised. A manual valve is mounted in parallel to the back-pressure regulator to allow for pressure letdown at the end of an experiment. As a safety precaution, an over-pressure relief valve has been mounted between the reactor exit and solenoid valve 6. This valve will release gas to vent if the reactor pressure rises above 4,220 kPa.

All equipment and tubing in contact with hydrogen or synthesis gas are constructed of either 304- or 316- stainless steel. Regulators and tubing coming in contact with only helium or nitrogen are made of brass. In general, all tubing is 316- stainless steel 1/4-inch O.D. with 0.035-inch wall thickness. The maximum safe working pressure of this system at 21°C is approximately 7,000 kPa.

#### 4.1.1.2 Vibrofluidized-Bed Microreactor

Figure 4.2 and 4.3 are cross-sectional schematic diagrams of the vibrofluidized-bed microreactor used for steady-state Fischer-Tropsch experiments. This microreactor consists of three sections: (1) the base section; (2) the reaction section; and (3) the product-exit section.

As shown in Figures 4.2 and 4.3, the base section consists of a 6.35-mm hole drilled through a solid, cone-shaped piece of 316-stainless steel. A 1/4-inch O.D. tube with 0.035-inch wall thickness was slid through this hole and welded in place. Starting in the center of the flat, top surface of the base section, a 3.175-mm wide slot was milled down through the 1/4-inch tube. This slot extends 12.7 mm in each direction from the centerline and in line with the 1/4-inch tube. A wider, 6.35-mm slot was milled in the same fashion, but only 1.588-mm deep. This second slot allows a sintered stainless-steel distributor plate to be recessed into the base section of the microreactor. The gas space below the distributor plate is termed "the plenum zone."

Other features of the microreactor base section include an O-ring groove and threaded holes to receive connecting bolts. Two guide rods

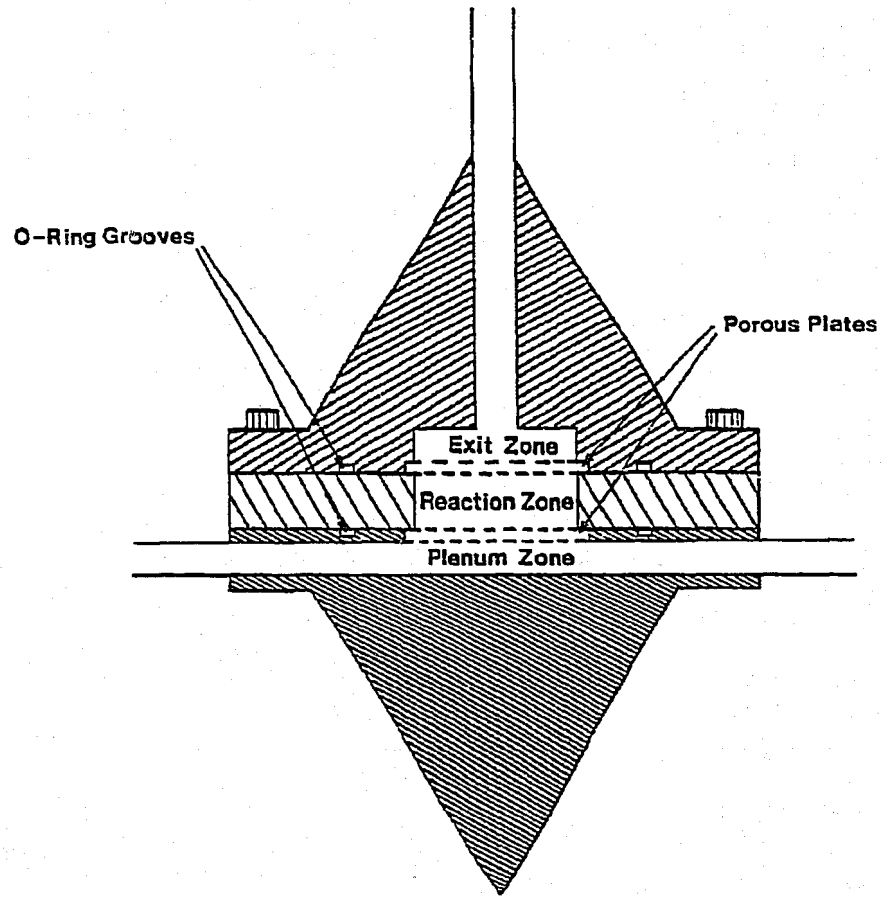


Figure 4.2. A Cross-Sectional Schematic Diagram of the Vibrofluidized-Bed Microreactor (front view).

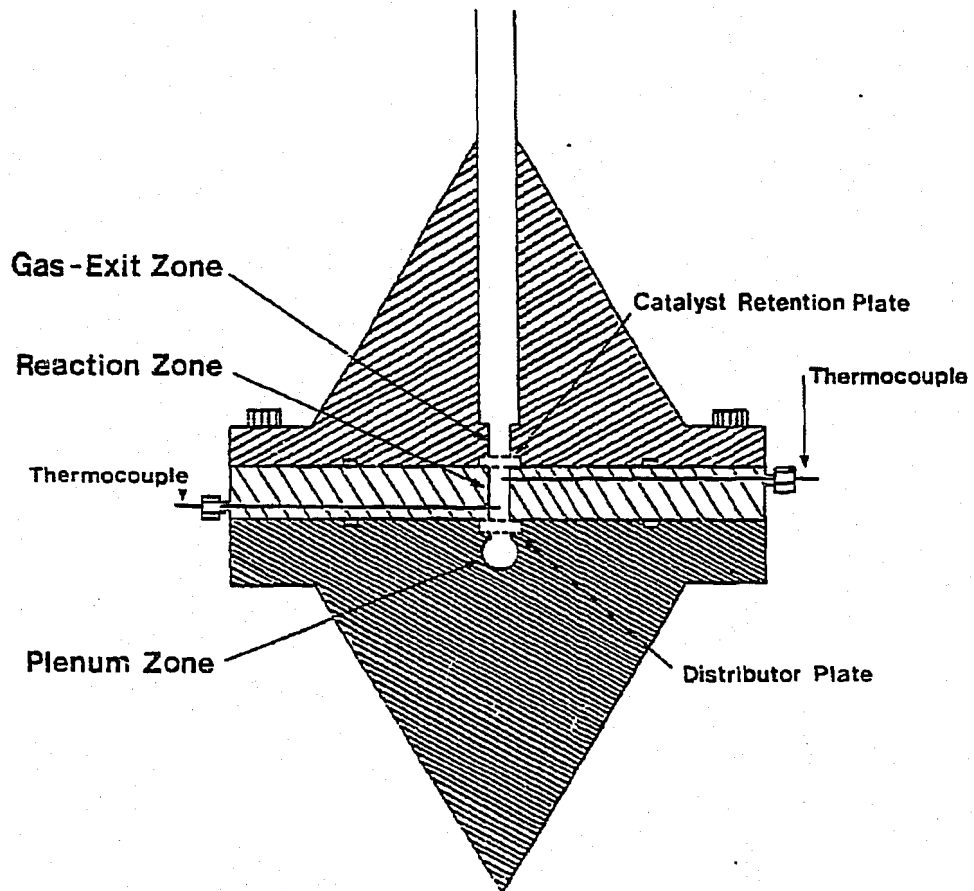


Figure 4.3. A Cross-Sectional Schematic Diagram of the Vibrofluidized-Bed Micro-reactor (side view).

press fitted into the base section facilitate alignment of the reaction section and the product-exit section.

The reaction section consists of a 14.29-mm thick, 316- stainless-steel disk, 63.5 mm in diameter. A 3.175-mm by 25.4-mm slot or "reaction zone" has been milled through the center of the disk. Two 1.50-mm stainless-steel sheathed type J thermocouples extended into the center of the reaction zone. The first is mounted 3 mm above the distributor plate while the second is 3 mm below the top of the reaction zone.

The final section of the microreactor, the product exit section, is a solid piece of 316- stainless steel in the form of an inverted cone. A slot, 25.4-mm long by 3.175-mm wide by 6.35-mm deep, has been milled in the flat surface to match the slot cut in the reaction section. A recess identical to the one milled into the base section holds a sintered stainless-steel catalyst retention plate. This plate keeps the catalyst from blowing out of the reaction zone during periods of high gas flow rate, for example, during purging. A vertical 1/4-inch O.D. stainless-steel tube with a 0.035-inch wall thickness passes down through the centerline of the product-exit section and connects with the milled slot.

During F-T synthesis experiments, gas first passes into the plenum zone, where it flows up through the distributor plate into the bed of vibrofluidized catalyst particles. Product gases and unreacted feed gases then flow through the catalyst retention plate and out of the reactor via the product-exit section. The reaction zone was designed as a slot, rather than a cylinder, in order to provide a maximum heat-transfer area. In addition, a reaction zone in the form of a slot provides for no dead volume in the reaction zone. The latter provision becomes extremely

important when rapid gas cycling is desired. This will be discussed further below in connection with unsteady-state F-T synthesis experiments.

This microreactor must remain leak-tight at temperatures up to 450°C and pressures to 2,229 kPa. Conventional gasket materials can not withstand these severe conditions and therefore metal O-rings must be used. A silver-plated stainless-steel O-ring (American Seal and Engineering Company) was used (1) between the reaction section and base section and (2) between the reactor section and product-exit section of the microreactor. Grooves in the base and product-exit sections of the microreactor accept these O-rings.

The three microreactor sections are bolted together using eight 1/4-20 hardened bolts. The O-rings are smashed into their grooves and gas pressure acts to force the ring against the metal, sealing the reactor. New O-rings are used for each experiment and provide enough sealing power to prevent even hydrogen from leaking. A "Grafoil" gasket, manufactured by Union Carbide, is used around the edges of the distribution plate to prevent the possibility of feed gas bypassing the distributor by going around its edges. The exterior shape of the microreactor is conical in order to promote the breaking of gas bubbles in the fluidized constant-temperature bath. This, in turn, provides for better bath-to-reactor heat transfer and promotes more vertical vibration of the microreactor.

#### 4.1.1.3 Vibrating System

Figure 4.4 is a schematic diagram of the vibrating and suspension system of the microreactor. The microreactor is suspended down into the constant-temperature bath by four threaded rods. These rods are bolted to a 101.6-mm square plate, 6.35-mm thick. This square is attached to a support structure by four 177.8-mm long leaf springs, 25.4 mm wide. Each spring consists of two 1.59-mm thick tempered spring-steel leaves. A single threaded bolt connects the square reactor support in the center of the leaf springs to the vibrator. The vibrator is securely anchored to the wall through the use of an I-beam. It was found that support systems with a smaller mass than the I-Beam tended to resonate. The vibrator itself is manufactured by Ling Dynamic Systems (model V203). The maximum peak-to-peak amplitude for this unit is physically limited to 6 mm. The vibrator is driven by a function generator (Wavetek model 182A) with an inhouse-constructed amplifier. The microreactor is typically operated at the resonance frequency of the leaf-spring support structure. This is generally between 18 and 24 Hz.

#### 4.1.1.4 Product Sampling System and Gas Chromatographic Analysis

In the steady-state vibrofluidized-bed microreactor system, F-T synthesis products and unreacted feed gases are continuously drawn through gas sampling valves for gas chromatographic analysis. Figure 4.5 is a schematic diagram of the product sampling and analysis systems. The major components of this system include: (1) two Valco sampling valves, a six-port and a ten-port valve; and (2) a gas chromatograph (Hewlett Packard 5730A). Product gases (P) are drawn from the



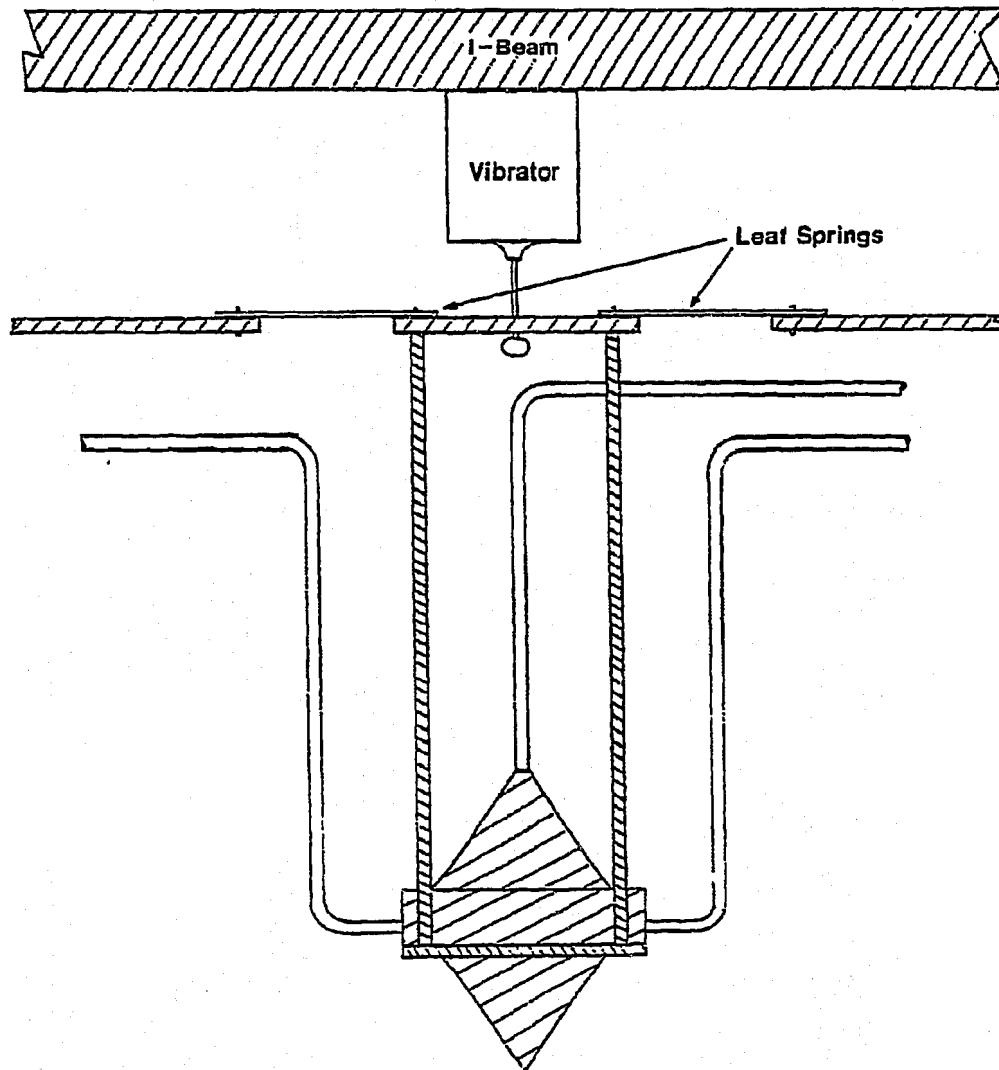


Figure 4.4. A Schematic Diagram of the Micro-reactor Vibrating and Suspension System.

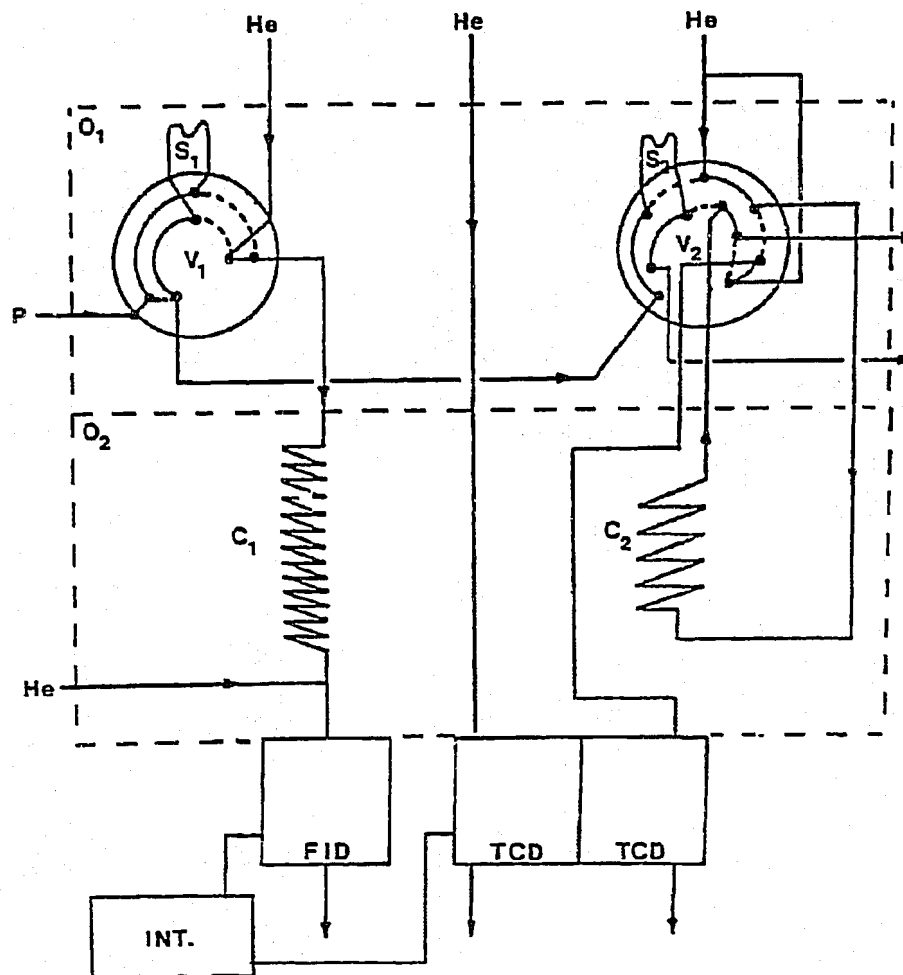


Figure 4.5. A Schematic Diagram of the Product Sampling and Analysis Systems in the Backflush Mode. Refer to Figure 4.1b for an Explanation of Equipment Symbols.

high-pressure reactor system at 50 standard mm<sup>3</sup> per second through a double-needle valve through which the pressure is reduced to nearly atmospheric pressure. The gases pass through a 1/16-inch O.D. tube to the two high-temperature Valco sampling valves.

Both the tubing and the sampling valves are maintained at 200°C (O<sub>1</sub>) through the use of direct metal-contact heating cords with an insulating tape. The heating cords are regulated by three variacs. The first sampling valve (V<sub>1</sub>) is a 6-port valve for injecting 0.03-ml samples into a 60-m fused-silica capillary column (C<sub>1</sub>) with a (J&W Scientific Durabond DB-1) 0.25-micron film thickness. This column is connected to a flame ionization detector (FID) for analysis of C<sub>1</sub> to C<sub>10</sub> hydrocarbons as well as some oxygenated compounds. The other sampling valve (V<sub>2</sub>) is a 10-port valve for injecting 0.2 ml samples into a 6-ft Analabs Spherocarb 80/100-mesh packed column (C<sub>2</sub>). This column is connected to the thermal conductivity detector (TCD) of the gas chromatograph for detection of light gases, including CO, CO<sub>2</sub>, methane and argon (which serves as an internal standard).

Figure 4.5 shows the normal position of the sampling valves and the usual gas flow path. Helium flows continuously through the capillary column (C<sub>1</sub>) in the forward direction, while the packed column (C<sub>2</sub>) is backflushed. Backflushing the packed column removes higher-molecular-weight species that have adsorbed on the front of the column during the previous 10-port valve sampling.

Figure 4.6 shows both sample valves (S<sub>1</sub> and S<sub>2</sub>) flushing samples into their respective columns. Samples are taken automatically using a Heathkit H-89 microcomputer, which is interfaced to the air-actuated

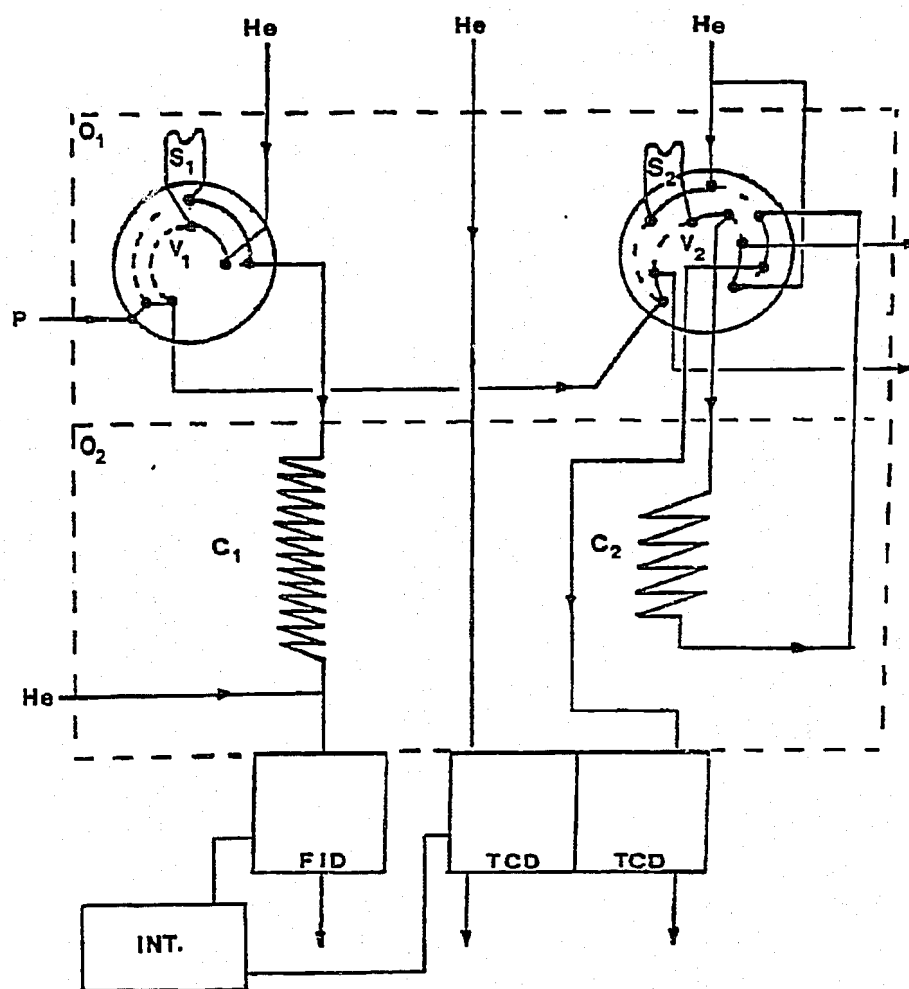


Figure 4.6. A Schematic Diagram of the Product Sampling and Analysis Systems in the Sampling Mode. Refer to Figure 4.1b for an Explanation of Equipment Symbols.

Valco sampling valves. Sample valve  $V_1$  is switched to the position shown in Figure 4.6 only momentarily allowing sufficient time for the sample to be flushed from the sample loop into the capillary column. Conversely, sample valve  $V_2$  remains in the pictured position until the last peak of interest ( $CO_2$ ) elutes.

Gas sampling valves,  $V_1$  and  $V_2$ , can be actuated simultaneously, flushing identical samples into the columns which, in turn, yields quantitative information on all major species of interest except hydrogen and water. Accurate amounts of carbon-containing species can be determined by relating the weighted argon peak-area on the packed-column chromatogram to the percent argon in the premixed synthesis gas and to the synthesis-gas flow rate. A methane peak appears on both chromatograms and serves as a basis for equating the analysis of species in both chromatograms. In this way, it is possible to determine quantitatively the carbon monoxide conversion and the carbon number distribution of the products.

In practice, simultaneous packed and capillary column samples are rarely taken. The short duration (on the order of hours) of F-T carbon-deposition experiments does not allow for complete analyses. This is because it takes over an hour for a temperature-programmed capillary sample to elute from the column. In the present work, isothermal ( $70^\circ C$ ) light gas samples are normally taken once every 37 minutes and only one capillary analysis is done at the conclusion of the experiment. These 37-minute cycles of light-gas sampling are made up of a 17-minute period for peak elution followed by a 20-minute backflush period.

Figure 4.7 is a typical light-gas chromatogram produced under isothermal (70°C) conditions and recorded using a recording integrator (Hewlett Packard model 3390A). The first peak to elute is hydrogen which can not be quantitatively detected using a pure helium carrier-gas because of their similar thermal conductivities. The remaining peaks are argon, carbon monoxide, methane and finally carbon dioxide. In order to quantify these peaks, thermal-conductivity weighting factors must be used.

Figure 4.8 is a typical product-gas chromatogram as separated by the fused-silica capillary column and detected by the flame ionization detectors. The chromatograph oven was held at -20°C for two minutes (using a liquid-nitrogen subambient unit) followed by temperature-programmed heating to 150°C at 4°C/min.

Major products have been identified through retention-time analysis and comparison to chromatograms obtained by Huff (1982), who employed a 50-m fused capillary column similar to the one used here. The first peak is actually two peaks, which overlap somewhat. The first of these overlapping peaks is methane while the second is a fused ethane-ethylene peak. C<sub>3</sub> olefins and paraffins also appear as a single fused peak. It should be noted that a pattern occurs for hydrocarbon elution. Normal-alpha-olefins of a given carbon number, C<sub>n</sub>, elute first in the greatest quantity followed by a lesser amount of normal paraffins of carbon number C<sub>n</sub>. Finally, beta-olefins elute in much smaller quantities.

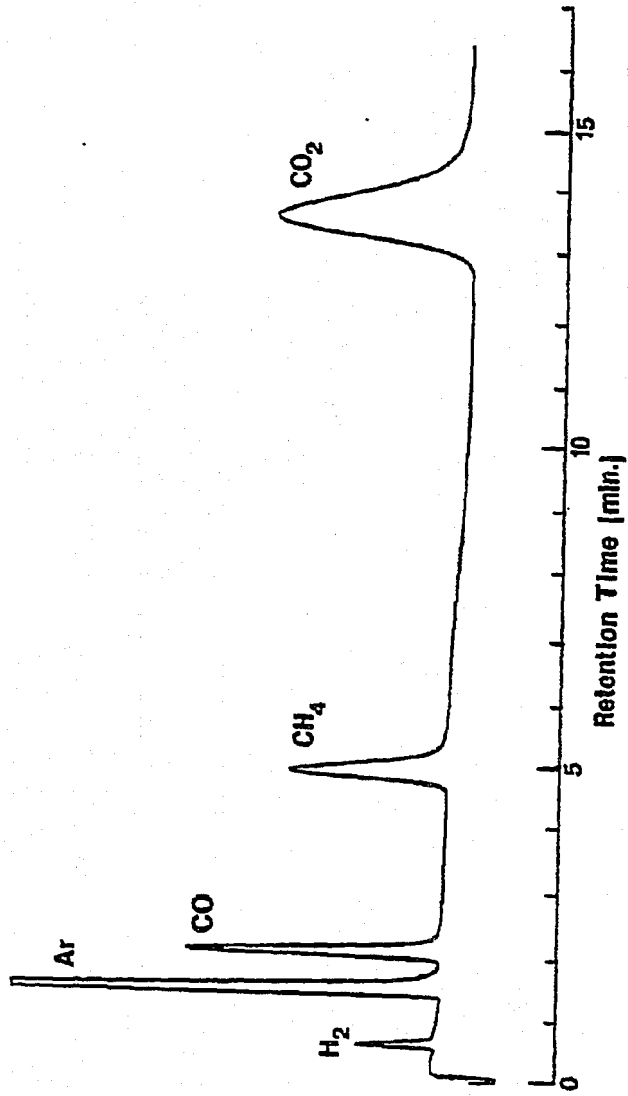


Figure 4.7. A Typical Light-Gas Product Chromatogram.

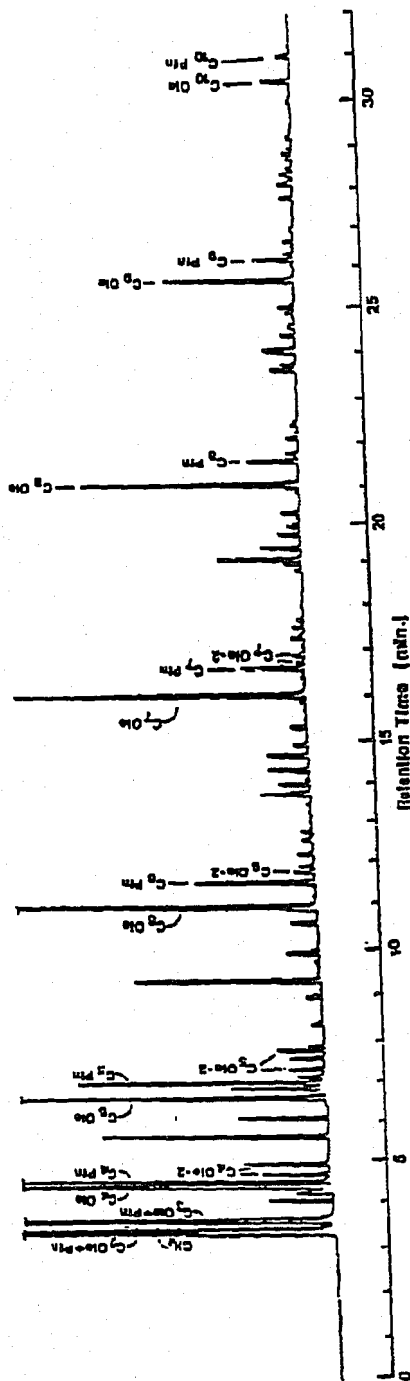


Figure 4.8. A Typical Product-Gas Chromatogram Separated on a Fused-Silica Capillary Column (Threshold is -2, Peak Width is 0.04, n-paraffins= Pfn, n-alpha-olefins=Ole, beta-olefins=Ole-2).



#### 4.1.2 Materials

##### 4.1.2.1 Catalyst

The catalyst used throughout the F-T studies is a commercial fused-iron ammonia-synthesis catalyst manufactured by United Catalysts, Incorporated. This catalyst is designated C-73-1-01 and has the composition shown in Table 4.1. The catalyst was originally supplied as granules, but has been crushed and sieved to a -150+300 micron fraction for these experiments. This size fraction provides for ease of vibrofluidization.

##### 4.1.2.2 Gases

Gases for system purging, catalyst reduction, and F-T synthesis were supplied by Airco-Industrial Gases, Research Triangle Park, NC. All carbon monoxide was supplied as C.P. grade; while hydrogen, argon, helium and nitrogen were prepurified grade. The trace impurities found in these gases are summarized in Table 4.2 as given by the manufacturer.

##### 4.1.2.3 Distributor and Catalyst Retention Plates

The distributor and catalyst retention plates used in this study were made by sintering 316- stainless-steel powder. The manufacturer, Mott Metallurgical Corporation, differentiates the filtering capabilities of the plates through the use of "micron-filter grades." The filtration grade in units of microns corresponds to the nominal spherical particle retention of the plate if it did not have a tortuous path. The actual particle size retention is much smaller than the filtration grade because of the porous matrix of the sintered plates. In subsequent discussions, the plates will be referred to by their filtration grade.

TABLE 4.1

Chemical Analysis and Physical Characteristics of  
Fused-Iron Catalyst C73-1-01

---

Item	Amount
1. Composition	
FeO	30-37%
Fe <sub>2</sub> O <sub>3</sub>	65-58%
Free Fe	< 0.5%
Total Fe	67-69%
Al <sub>2</sub> O <sub>3</sub>	2.0-3.0%
K <sub>2</sub> O	0.5-0.8%
CaO	0.7-1.2%
SiO <sub>2</sub>	< 0.4%
P	< 0.015%
S	< 0.001%
Cl	< 0.002%
Fe <sup>++</sup> /Fe <sup>+++</sup>	0.45-0.65%
2. Bulk Density	2723 ± 160 kg/m <sup>3</sup>

---

TABLE 4.2

## Purity of Feed and Purge Gases

	CO	H <sub>2</sub>	Ar	He	N <sub>2</sub>
Minimum Purity %	99.3	99.995	99.998	99.995	99.995
Total Maximum Impurities (ppm)	-	50	20	50	50
Maximum Individual Impurities (ppm)					
Ar	-	-	-	-	35
H <sub>2</sub>	-	-	2	2	2
N <sub>2</sub>	1500	20	10	20	-
O <sub>2</sub>	600	5	2	6	1
CO + CO <sub>2</sub>	50	2	2	2	0.5
THC	-	5	2	0.5	0.5
H <sub>2</sub> O	-	8	-	10.0	10
He	-	-	5	-	10

### 4.1.3 Experimental Procedure

#### 4.1.3.1 Microreactor Cleaning and Catalyst Charging

Before each experiment, the mating surfaces of the three sections (see Figures 4.2 and 4.3) of the microreactor were polished with  $\Delta 600$  emory cloth on a surfacing table. The reactor was then flushed thoroughly with acetone and wiped with Kimwipes. Particular attention was focused on the reaction zone. After cleaning, the base section of the microreactor was clamped in a vise using a wooden support apparatus. A new 20-micron distributor plate was then weighed and inserted into the recessed slot in the base. A small oval-shaped Grafoil gasket was then placed around the mating edges of the distributor plate and the base. A new silver-plated stainless-steel O-ring was placed in the O-ring groove of the base section.

The reaction section of the microreactor was then slipped down over the guide rods of the base section. One gram of the  $-150+300$  micron fused-iron catalyst was then weighed and poured into the reaction zone. A 40-micron catalyst retention plate was placed into the recess in the product-exit section. In addition, a new O-ring was placed in the O-ring groove in this top section. The product-exit section was slid down over the guide rods coming to rest on top of the reaction zone.

The sections were then bolted together using eight hex-head bolts. These bolts were tightened in an alternating pattern one-half turn at a time and then torqued to 27 N-m with a torque wrench. The 1/4-inch O.D. tubes of the microreactor were then temporarily capped off to prevent the reactor from being contaminated.

#### 4.1.3.2 Mounting of the Microreactor

Following catalyst loading, the microreactor had to be attached to the vibrational support system. A yoke was bolted to the base section of the microreactor. Four 1/4-inch threaded rods were then screwed into the yoke. This support and the microreactor were slipped down into the fluidized constant-temperature bath. The threaded rods were then bolted to the leaf-spring supports. The three 1/4-inch O.D tubes leading to the microreactor were attached to the flexible stainless-steel hoses using compression fittings. This effectively connected the microreactor to the remainder of the system.

Finally, the vibrator itself was mounted to the underside of the I-beam support and connected to the microreactor support system (see Figure 4.4). The vibrational frequency of the frequency generator was then adjusted to the point where the microreactor was vibrating at the maximum amplitude. This corresponded to a resonance frequency of 18-24 Hz with a microreactor peak-to-peak amplitude of 4 mm.

#### 4.1.3.3 System Startup and Catalyst Reduction

The reader is suggested to refer to Figure 4.1a for the following discussion. Before system startup, the portion of the system located downstream of solenoid valves 1-4 was flushed thoroughly with helium. This was done by opening valves V4 and V9, and solenoid valves 5 and 6, and then directing three-way valves V6, V7, and V8 so that helium flows through the system. The portion of the system located upstream of solenoid valves 1-4 was normally kept under pressure. This upstream portion therefore need only be purged after changing out a gas cylinder.

After the system has been purged with helium, solenoid valves 5 and 6 were closed and the microreactor was checked for leaks at 3,435-kPa helium atmosphere. Valve V9 was closed so that all exiting gas must go through the back-pressure regulator or the sampling valves. The pressure upstream of solenoid valves 1-4 was set to 4,807 kPa using the two pressure transducers. These transducers were then switched to read gas pressures downstream of the microreactor by turning the appropriate three-way valves.

The nitrogen ballast gas was introduced to the back-pressure regulator by opening valve V1. The system pressure downstream of the microreactor was then set to 2,210 kPa by adjusting the nitrogen ballast gas pressure and flow along with the back-pressure regulator setting.

Once the system pressure had been set, the flow rates of reducing gas, precarburization and main reaction synthesis gases could be set. First, the flow rate of synthesis gas was set using the needle valve associated with solenoid valve 2. This was performed by first purging the system with synthesis gas through opening solenoid valves 1, 2, 5 and 6 and letting gas flow through the reactor at  $6.7 \times 10^4$  standard  $\text{mm}^3$  per second for one minute. Solenoid valves 1 and 5 were shut and synthesis gas passed solely up through the microreactor reaction zone. The flow rate of synthesis gas was finally set by adjusting the needle valve associated with solenoid valve 2, while monitoring the flow rate using the flow transducer.

Precarburization synthesis gas originated in the center cylinder shown in Figure 4.1a. The flow rate of this gas was set in a similar

fashion to that described above for the reaction synthesis gas. Solenoid valves 5 and 6 were opened and the reactor was purged with precarburization synthesis gas. After one minute of purging at a flow rate of  $6.7 \times 10^4$  standard  $\text{mm}^3$  per second, valve 5 was closed and the flow rate through the reactor was set by adjusting the needle valve before three-way valve V7. Finally, the gas flow rate of reducing hydrogen was set using the needle valve associated with solenoid valve 4, after sufficient purging of the reactor had been completed.

The hydrogen flow path consisted of gas flowing through valves V5 and V8 in conjunction with solenoid valves 4 and 6. At this point, the reduction period was nearly ready to be started. Air was started to the fluidized constant-temperature bath, and the bath temperature-controller along with the variacs controlling the heating cords were switched on. The microreactor was started vibrating and the gas chromatograph was set up.

The reduction period consisted of a 2.5-hour bath heat-up period followed by a 6-hour isothermal duration at  $450^\circ$ . The hydrogen flow rate during reduction was 3,670 standard  $\text{mm}^3$  per second.

#### 4.1.3.4 Precarburization and Steady-State Synthesis

Precarburization was used in order to convert the fused-iron catalyst to Hägg carbide without excessive carbon deposition. A higher ratio of hydrogen to carbon monoxide is used for precarburization (about 4:1) than that for reaction during steady-state synthesis. After the reduction period had been completed, the catalyst was first exposed, in some cases, to the precarburization synthesis gas for two hours. This

precarburization step was followed by exposure of the carburized catalyst to the reaction synthesis gas of a lower  $H_2/CO$  ratio. The exposure to the synthesis gas of a lower  $H_2/CO$  ratio initiated carbon deposition.

Precarburization was initiated by closing solenoid valve 4 (shutting off the  $H_2$ -flow) and switching three-way valves V6, V7, and V8 so that precarburization gas flowed through the microreactor. The flow rate of this gas had been previously set, so no needle-valve adjustment was necessary.

Immediately after the start of precarburization synthesis-gas flow, a timing computer-program was started using the Heathkit H-89 microcomputer. After the first twenty minutes of precarburization synthesis, a product gas sample was flushed into the packed column of the gas chromatograph automatically by the computer-actuated sampling valves. Seventeen minutes after the product gas sample was taken, all compounds of interest had eluted and the computer backflushed the heavy products from the packed column. This process was repeated every 37 minutes throughout the precarburization and synthesis portions of the experiments. The course of the reaction can be monitored through the use of the two thermocouples in the reaction zone. The exothermicity of the F-T synthesis reaction showed up typically several minutes after the precarburization synthesis gas starts flowing. It takes this long for the new gas to replace hydrogen in the reactor feed-lines.

After two hours of precarburization with  $H_2/CO$  gas of a 4:1 ratio, the catalyst was sufficiently carburized and the steady-state synthesis



period began with a synthesis gas of a low H<sub>2</sub>/CO ratio. The precarburization synthesis gas was shut off and reaction synthesis gas was started by switching three-way valve V7 and opening solenoid valve 2. Automatic product gas sampling was continued and the experiment proceeded for the specified amount of time.

Several minutes before the end of an experiment, the gas chromatograph oven was cooled down to -20°C with liquid nitrogen and a sample was manually flushed into the capillary column. A sample could not be in the packed column while the oven was cooling because the baseline changed with temperature. After the sample had been flushed into the capillary column, the temperature program and the integrator were started. The system could be shut down without any effect on the gas chromatograph.

#### 4.1.3.5 System Shut-Down

After the synthesis period was completed, it was desirable to shut down the system as rapidly as possible, while blanketing the catalyst in an inert gas. This was done by flushing the catalyst and the microreactor system lines with helium and rapidly reducing the system to atmospheric pressure. Synthesis was stopped and flushing was started by shutting solenoid valve 2 and immediately directing three-way valves V6 and V7 towards the helium cylinder. The nitrogen ballast flow was shut off using valve V1, and vent valve V9 was opened slowly over the course of several minutes. It is important that vent valve V9 not be opened too rapidly. Otherwise, gas will pass through the reaction zone

at a velocity high enough to plaster the catalyst against its retention plate. The flow rate of gas through the reaction zone should be maintained below 2,200 standard  $\text{mm}^3$  per second in order to prevent this. Yet the flow rate should be high enough to prevent condensation of residual F-T products.

Once the system had been purged with helium and had reached atmospheric pressure, the temperature controller to the constant-temperature bath was shut off. The vibrator and the heating tapes were left on until the system had cooled. The cool-down period typically lasted five hours after which the vibrator and heating tapes were shut off.

#### 4.1.3.6 Catalyst Collection and Analysis

After the microreactor had been cooled to ambient temperature, it was removed from the constant-temperature bath. The microreactor was detached from the flexible stainless-steel hoses and the helium flow was stopped. The tubes leading to the microreactor were capped and it was dismantled from the suspension apparatus.

Following removal from the bath, the reactor was clamped into a vise, where the exterior was cleaned and the connecting bolts were removed. The top or product-exit section was then removed and carefully placed aside, taking care not to lose any carbon fines that may have been sticking to the catalyst retention plate. If all had gone well during the reaction, the catalyst in the reaction zone was free flowing (not sticky) and maybe darkened somewhat by carbon deposition. The catalyst was then extracted from the reaction zone using a suction-filter

apparatus. The latter consisted of a pasture pipet, a piece of filter paper, some tygon tubing, a filter flask and an aspirator. The catalyst was drawn up into the pipet by suction, and any fine carbon powder or "bugdust" was collected on the filter paper. The heavier catalyst was then dumped into a vial by releasing suction. The bugdust was placed in a second vial by tapping the pipet gently.

An additional accumulation of bugdust was sometimes found pressed against the catalyst retention plate. This accumulation was removed by the suction-filter apparatus and added to the bugdust vial. By weighing the vials and the filter apparatus before and after, an accurate determination of the disposition of the spent catalyst was made. Furthermore, any weight gain experienced by the catalyst retention plate was considered bugdust.

The spent catalyst and bugdust vials were purged with nitrogen and portions were mailed to Gailbiarth Laboratories, Knoxville, TN where carbon and iron analyses were performed. Other select samples were sent to the Physics Department at West Virginia University where Mössbauer spectroscopic studies of the iron phases were undertaken.

#### 4.2 Experimental Results and Discussion

The results of steady-state synthesis runs are presented in this section. The aim of these studies was twofold. First, conditions had to be found where production and condensation of liquid products and/or waxes on the catalyst surface did not affect catalyst vibrofluidization. Secondly, carbon deposition data had to be obtained for feed gases of

several different  $H_2/CO$  ratios under conditions where the catalyst would not defluidized.

Table 4.3 gives a summary of experimental conditions and results for pertinent steady-state runs applicable to the catalyst defluidization studies. Similarly, Table 4.4 lists the experimental conditions and results for the steady-state carbon-deposition runs. The letter assigned to a particular run number designates a particular reaction temperature, while the associated number indicates the chronological order of the experiments. Several of the steady-state catalyst defluidization experiments in Table 4.3 are also applicable to the carbon deposition studies listed in Table 4.4.

In addition, many other steady-state runs were performed before these experiments. These earlier experiments led to the present vibrofluidized-bed microreactors design. The history of this development is documented in Appendix E. Appendix B provides a compilation of primary and secondary results from steady-state experimental runs. For each run, the CO conversion as well as the  $CO_2$  and  $CH_4$  produced are presented as a function of time. In addition, a derived mass balance allows an approximate mass balance to be performed. The results of the balance are also listed.

#### 4.2.1 Catalyst Defluidization

Vibrofluidized fused-iron catalysts for F-T synthesis have been found to be subject to defluidization. The reason for the loss of fluidity has been proven in earlier studies undertaken in this

TABLE 4.3

A Summary of Steady-State Results and Run Conditions for Vibrofluidized-Bed  
Microreactor Defluorination Studies

Run Number	Duration of Synthesis hours; min.	H <sub>2</sub> /CO Feed Gas Ratio	Temperature °C	Total Pressure kPa	Catalyst Charged, g	Distributor Plate Opening, $\mu$
B-1	10; 0	2.08	360	2220	1.0077	20
B-2	2; 3	2.08	360	2220	1.0077	20
B-3	10; 0	4.0	360	2220	1.0168	20
B-4	1; 2	1.03	360	2220	1.0176	40
B-5	2; 13	1.03	360	2220	1.0060	40
B-6	2; 57	2.08	360	2220	1.0020	40
B-7	2; 45	2.08	360	2220	1.0030	20
C-1	2; 4	2.08	400	2220	1.0089	20
C-2	1; 0	1.03	400	2220	1.0175	20
D-1	1; 15	1.03	380	2220	1.0135	20
D-2	2; 48	2.08	380	2220	1.0053	20
E-1	2; 50	2.08	390	2220	1.0479	20

TABLE 4.3 (Continued)

Distribution of Spent Catalyst After Run, g

Run Number	Free Flowing	Defluidized	Bugdusted (Carbon Powder)	Net Weight Change of Reaction-Zone Material, mg	Comments
B-1	-	1.3007	-	+369.3	Black, Sticky
B-2	0.7417	-----> 0.1980	-----	-62.8	Unclear
B-3	0.6407	0.6320	-	-63.7	Somewhat sticky, no bugdust
B-4	0.9260	-----> 0.0111	-----	-71.0	Unclear
B-5	0.1315	0.8945	-	+56.5	Sticky
B-6	0.1484	0.7852	-	-52.6	Sticky
B-7	-	0.9569	-	+45.9	Sticky
C-1	0.9629	-	0.0510	+10.4	Bugdust
C-2	-	-	1.1492	+146.4	Totally bugdust
D-1	0.9027	-	0.1258	+18.1	Bugdust
D-2	0.5762	-----> 0.4615	-----	+51.1	Unclear
E-1	0.8685	-	0.2628	+83.4	Bugdust

NOTE: The space velocity was 34,320 hr<sup>-1</sup> for all runs listed in this table.

TABLE 4.4  
 A Summary of Steady-State Results and Run Conditions for Vibrofluidized-Bed Microreactor Carbon-Deposition Studies

Run Number	Duration of Synthesis, hours; min.	$H_2/CO$ Feed Gas Ratio	Catalyst Charged, g	Distribution of Spent Catalyst After Run, g			Net Weight Change of Reaction-Zone Material, mg	Comments
				Free Flowing	Defluidized	Bugdusted (Carbon Powder)		
F-1	3; 30	4.0	1.0039	0.9312	-	-	-72.7	No Bugdust
F-2	2; 0	4.0	1.0042	0.8901	-	-	-106.1	No Bugdust
F-3 (precarburization)	2; 0	4.0	1.0000	0.9046	-	0.0337	-61.7	Bugdust
	1; 0 (synthesis)	2.08						
F-4 (precarburization)	2; 0	4.0	1.0018	0.9524	-	0.0273	-22.1	Bugdust
	2; 0 (synthesis)	2.08						
F-5 (precarburization)	2; 0	4.0	1.0042	0.8971	-	0.0688	-38.3	Bugdust
	0; 22 (synthesis)	1.03						

Note: The following conditions were identical for all runs listed in the table: temperature = 395°C; pressure = 2,200 kPa; space velocity = 31,320 hr<sup>-1</sup>; and distributor plate type = 20a.

investigation. It is caused by the buildup of condensed liquid products and/or waxes in the catalyst pores, on the catalyst surface and, to a lesser extent, in the reaction zone.

In order to avoid defluidization in the vibrofluidized bed of  $-150+300 \mu$  catalyst particles, the product distribution must be shifted toward lower molecular-weight species. As explained in Section 2.2.5, the average molecular weight of products, represented by the probability of chain growth ( $\alpha$ ), can be altered by changing the synthesis conditions.

Runs B-1 through E-1 were a series of systematic experiments designed to identify a temperature at which future steady-state experiments could be performed in the vibrofluidized-bed microreactor without fear of catalyst defluidization. Preliminary experiments at lower temperatures produced a sticky catalyst mass and pointed to a reaction temperature of at least  $360^{\circ}\text{C}$  (see, for example, Runs B-1 to B-7, listed in Table 4.3). A complication to using high reaction temperatures is that carbon deposition becomes much more rapid as temperature increases. Dry (1981) states that for every 10K rise in bed temperature, a 50% increase in carbon deposition rate can be expected.

All defluidization experiments (Runs B-1 through E-1) consisted of catalyst reduction by hydrogen at  $450^{\circ}\text{C}$  and a space velocity of  $34,320 \text{ hr}^{-1}$  followed by reaction at the conditions listed in Table 4.3 (note that the space velocity is the volume of feed gas (standard  $\text{mm}^3$ ) fed per hour per volume of unreduced fused-iron catalyst. No precarburization step was used during these runs because of their exploratory nature.



Figure 4.9 shows the weight percent of catalyst that had defluidized as a function of reaction time for feed gases of three different  $H_2/CO$  ratios at  $360^\circ C$ . This temperature corresponds to the "B" series of experiments, B-1 through B-6.

For feed gases of  $H_2/CO$  ratios of 2:1 (Runs B-1, B-2, B-6, B-7) and 1:1 (Runs B-4 and B-5), defluidization of the vibrofluidized catalyst bed occurs after 2 to 3 hours of synthesis under the specified conditions. For a feed gas of a  $H_2/CO$  ratio of 4:1 (Run B-3), only approximately 42 percent of the catalyst has defluidized after 10 hours of steady-state synthesis.

During previous exploratory experiments, it was observed that a relationship existed between the degree of fluidity of the vibrofluidized catalyst bed and the temperature fluctuation at the lower thermocouple in the reaction zone. For each of the steady-state experiments, this fluctuation was observed and recorded periodically throughout the run. A typical observation involved watching the temperature output for 30 seconds and recording the difference between the high and low value. It was thought that the temperature fluctuation was induced by the vibration. The vibration caused periodic contact between the thermocouple and the catalyst particles where the highly exothermic reaction was taking place.

Figure 4.10 is a plot of the lower-thermocouple temperature fluctuation as a function of time for Run B-1 using a feed gas of 2:1  $H_2/CO$  ratio at  $360^\circ C$ . During the first two hours of the experiment, the temperature fluctuation ranged from  $0.6$  to  $1.0^\circ C$ . After three hours had

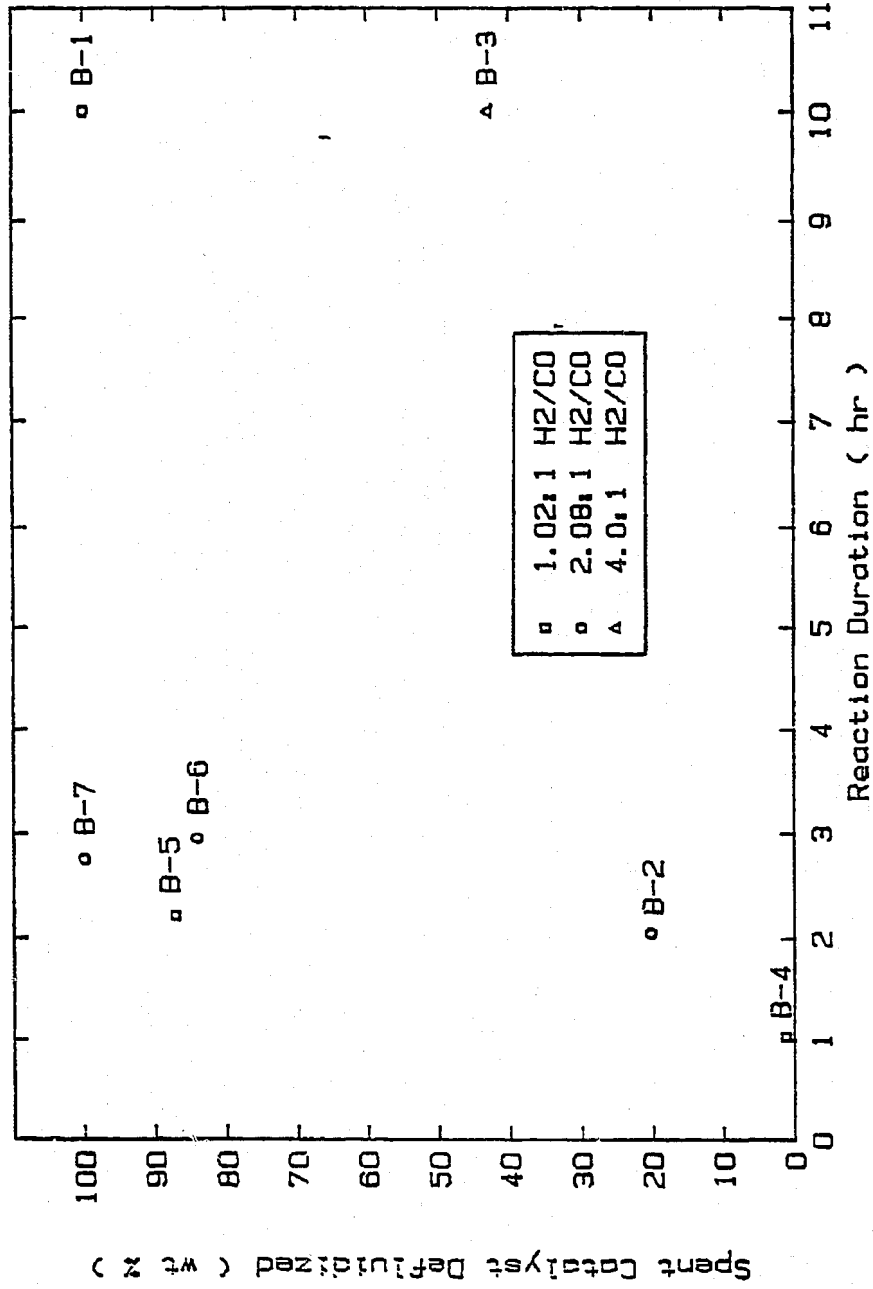


Figure 4.9. Defluidization Characteristics of Feed Gases of Three H<sub>2</sub>/CO Ratios at 360°C and 2220 kPa.

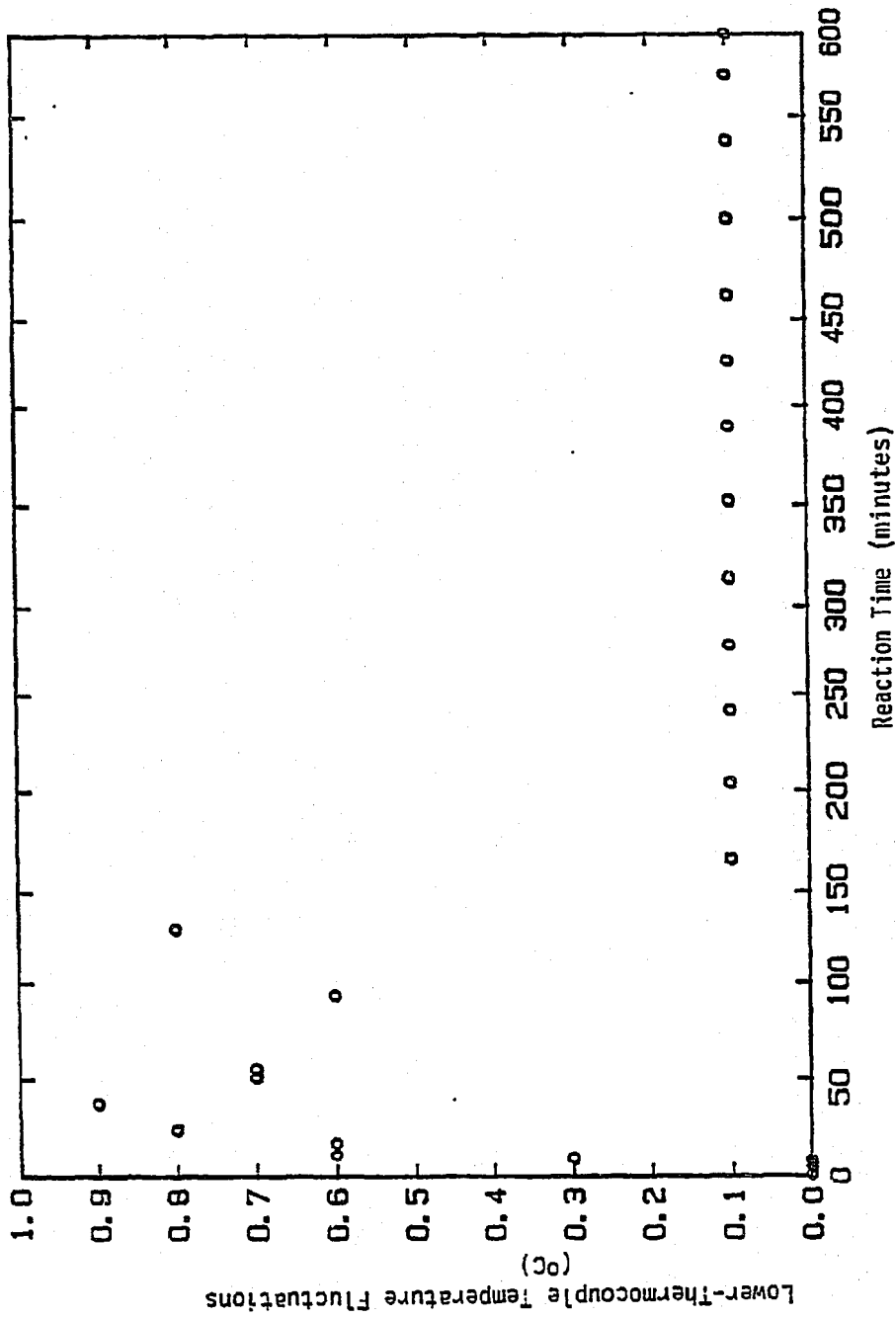


Figure 4.10. Lower-Thermocouple Temperature Fluctuation as a Function of Time for Run B-1 Using a Feed Gas of 2:1 H<sub>2</sub>/CO Ratio at 360°C and 2220 kPa.

elapsed, the fluctuation had dropped to  $0.1^{\circ}\text{C}$  and remained essentially constant. At this point, the catalyst bed was defluidized.

Figure 4.11, for Run B-7, gives a more detailed picture of the defluidization phenomenon in the vibrating microreactor. For 1.0 g of fused-iron catalyst at  $360^{\circ}\text{C}$  and 2,220 kPa and with a feed gas of 2:1  $\text{H}_2/\text{CO}$  ratio, the catalyst defluidized gradually over a period of about one hour. Similar plots of temperature fluctuation varying with time are given for Runs B-2 through B-5 in Appendix B.

Runs C-1 and C-2 were steady-state synthesis experiments performed, respectively, with feed gases of 2:1 and 1:1  $\text{H}_2/\text{CO}$  ratios at  $400^{\circ}\text{C}$ . The feed gas of 2:1  $\text{H}_2/\text{CO}$  ratio at this temperature did not cause the catalyst to defluidize during the two-hour run as reflected in Figure 4.12. Similarly, Run C-2 using a feed gas of 1:1  $\text{H}_2/\text{CO}$  ratio produced no defluidization after one hour, but carbon deposition was excessive. This will be further examined in Section 4.2.3.

Runs D-1 and D-2 were undertaken at  $380^{\circ}\text{C}$  using feed gases of 1:1 and 2:1  $\text{H}_2/\text{CO}$  ratios, respectively. The plots of temperature fluctuations as a function of time indicate catalyst defluidization after two hours and fifty minutes of operation.

Run E-1 involved raising the temperature to  $390^{\circ}\text{C}$  and repeating the defluidization study using a 2:1  $\text{H}_2/\text{CO}$  feed-gas ratio. Upon opening the microreactor after this run, the catalyst was found to be free flowing and very slightly sticky. When vacuumed up with the suction-filter apparatus, some of the catalyst stuck to the walls of the pipet. From Runs C-1 and C-2, it was known that the vibrofluidized catalyst would not defluidize before excessive carbon formation began at  $400^{\circ}\text{C}$ . Run E-1

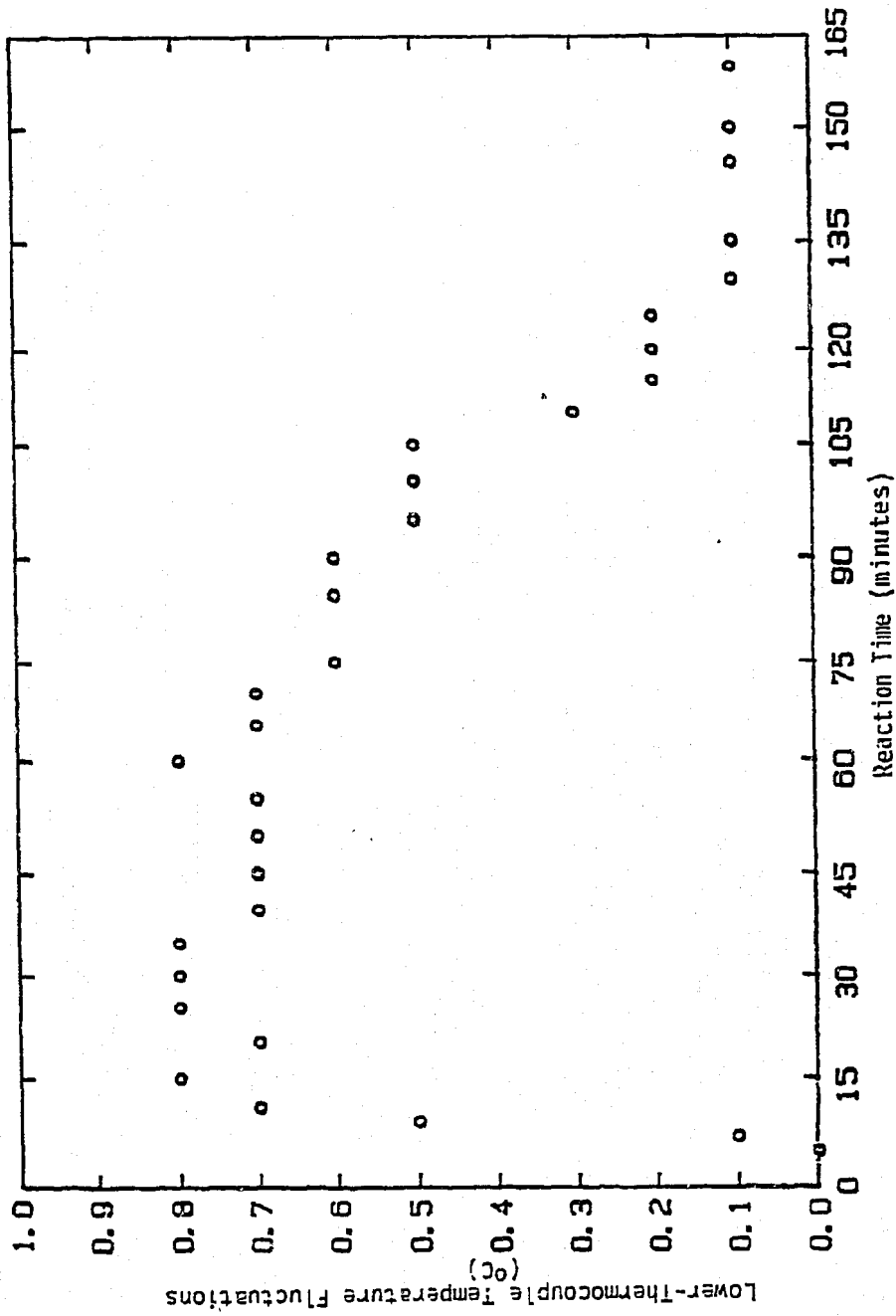


Figure 4.11. Lower-Thermocouple Temperature Fluctuation as a Function of Time for Run B-7 Using a Feed Gas of 2:1 H<sub>2</sub>/CO Ratio at 360°C and 2220 kPa.

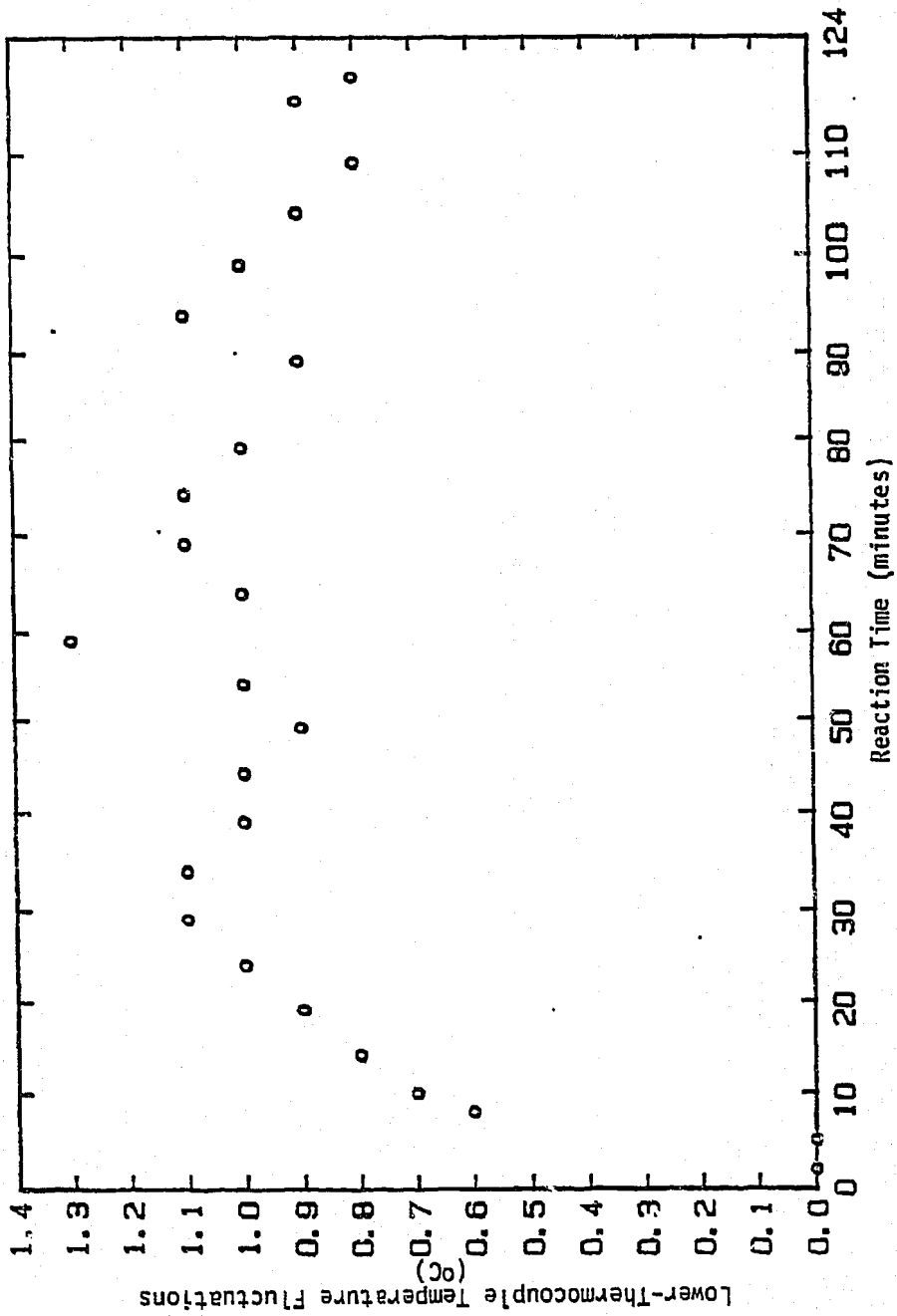


Figure 4.12. Lower-Thermocouple Temperature Fluctuation as a Function of Time for Run C-1 Using a Feed Gas of 2:1 H<sub>2</sub>/CO Ratio at 400°C and 2220 kPa.

indicated that the spent catalyst was only very slightly sticky after synthesis with a feed gas of 2:1 H<sub>2</sub>/CO ratio at 390°C. Consequently, it was concluded that an appropriate temperature for the steady-state carbon-deposition studies in the vibrofluidized-bed microreactors would be 395°C.

#### 4.2.2 Hydrocarbon Product Distribution

It has been explained in Section 2.1.5.3 that excluding oxygenated products in an analysis of the product distribution from a F-T synthesis run can cause inaccuracies. For instance, in a plot of the Flory distribution or Polymerization Distribution Law, Equation (4), Section 2.1.5, where the logarithm of the mole fraction of each product carbon number is plotted against the carbon number, significant deviations are observed for C<sub>2</sub> products. This is because approximately 20-30 percent of C<sub>2</sub> products for this iron catalyst are oxygenates (Huff, 1982). In order to provide an accurate Flory plot, it is necessary to carefully trap and separate product fractions, as well as to identify these fractions. The goal of the present study, however, was not to obtain these detailed data, but to observe general trends in product distribution as reaction parameters were changed.

Therefore, the on-line product analysis system described in Section 4.4.4.1 was utilized to obtain the distribution of C<sub>1</sub> to C<sub>10</sub> hydrocarbon products. Chromatographic analyses of hydrocarbon products were performed for selected steady-state experiments. The normal paraffin, normal alpha-olefin and beta-olefins for each carbon number up to C<sub>10</sub>

were considered when the peak could be identified. These results are listed in Appendix B.

During the compilation of the data, the weight fraction, mole fraction, and rate of production of each identified hydrocarbon species was determined. Figure 4.13 through Figure 4.16 show Flory plots for hydrocarbon products from Runs B-1, B-2, B-3, and C-1. As can be seen, a significant dip occurs at C<sub>2</sub> in all four plots. The reason for this is that a greater percentage of C<sub>2</sub> fraction products (20-30%) are oxygenates than for other carbon numbers.

The main points of interest in these plots are the slopes of the plots which represent the values of probability of chain growth,  $\alpha$ . Comparing Figure 4.13 (Run B-1) to Figure 4.15 (Run B-3), the probability of chain growth drops from 0.56 to 0.49. This result reflects the influence of the H<sub>2</sub>/CO ratio in the feed gas on  $\alpha$ . Run B-1 consisted of 10 hours of steady-state synthesis at 360°C and 2,220 kPa using a 2.08:1 H<sub>2</sub>/CO ratio. Run B-3 was an identical run except that a 4:1 H<sub>2</sub>/CO ratio was used. The difference between the results from Run B-1 (Figure 4.13) and Run B-3 (Figure 4.15) is consistent with existing Fischer-Tropsch data indicating that the product distribution shifts to lower molecular-weight products (smaller  $\alpha$ ), as the H<sub>2</sub>/CO ratio in the feed gas increases. On going to a higher reaction temperature, the probability of chain growth dropped. Run B-2 (Figure 4.14) consisted of approximately two hours of steady-state synthesis at 360°C and 2,220 kPa using a feed gas of 2:08:1 H<sub>2</sub>/CO ratio. Run C-1 (Figure 4.16) was identical to Run B-2, but was undertaken at 400°C. On going from 360°C to 400°C, the probability of



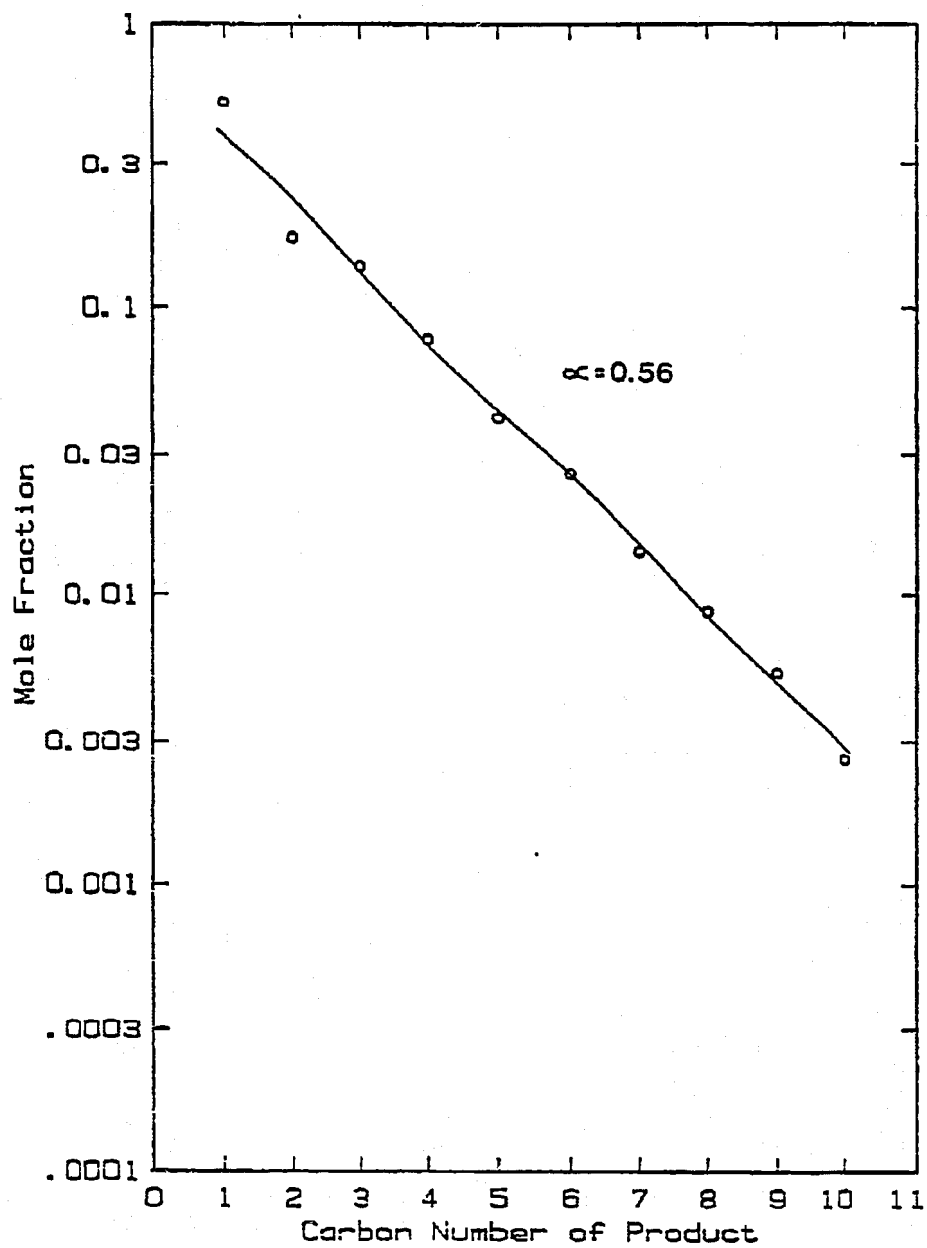


Figure 4.13. A Flory Plot of the Hydrocarbon Product Distribution from Steady-State Fischer-Tropsch Synthesis, Run B-1 (see Table 4.3 for Experimental Conditions).

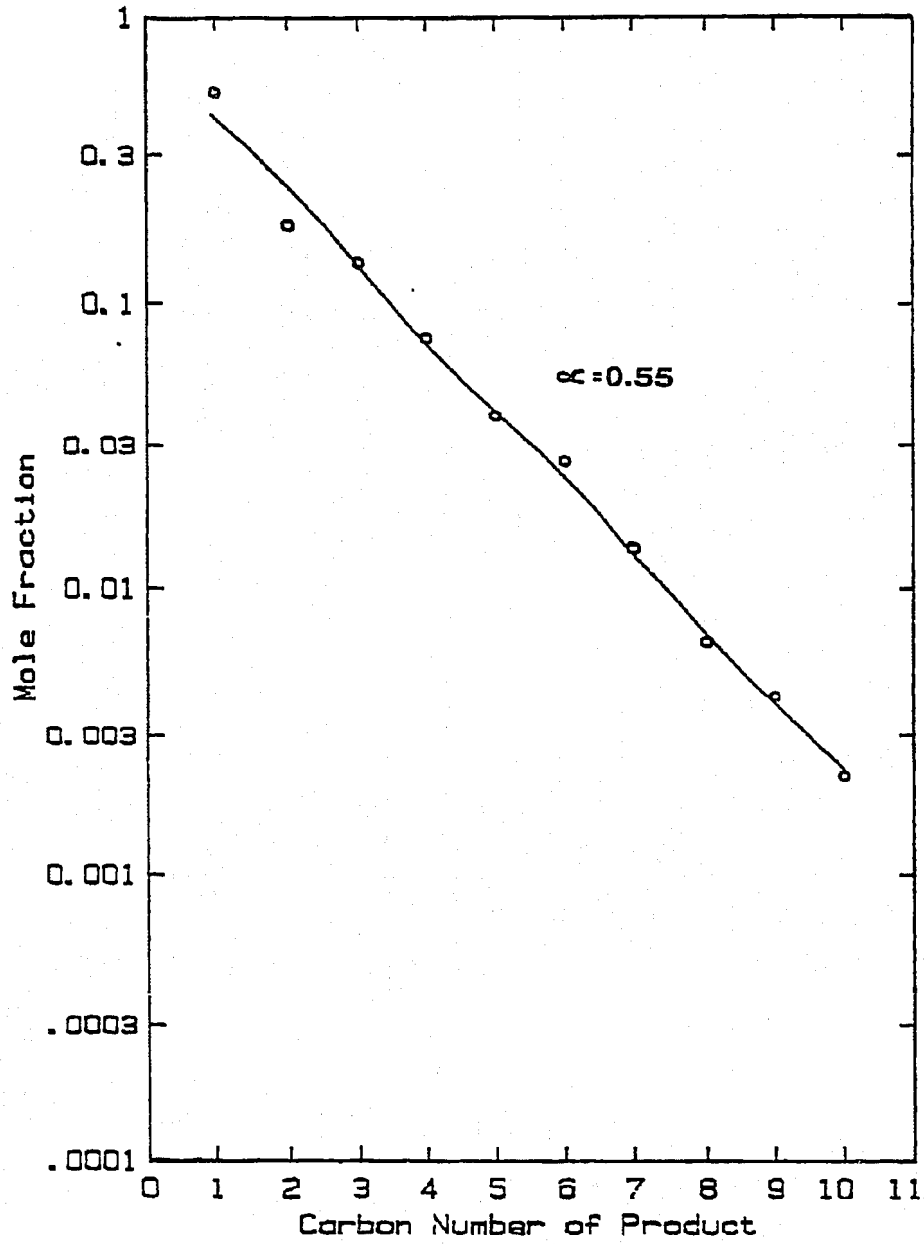


Figure 4.14. A Flory Plot of the Hydrocarbon Product Distribution from Steady-State Fischer-Tropsch Synthesis, Run B-2 (see Table 4.3 for Experimental Conditions).

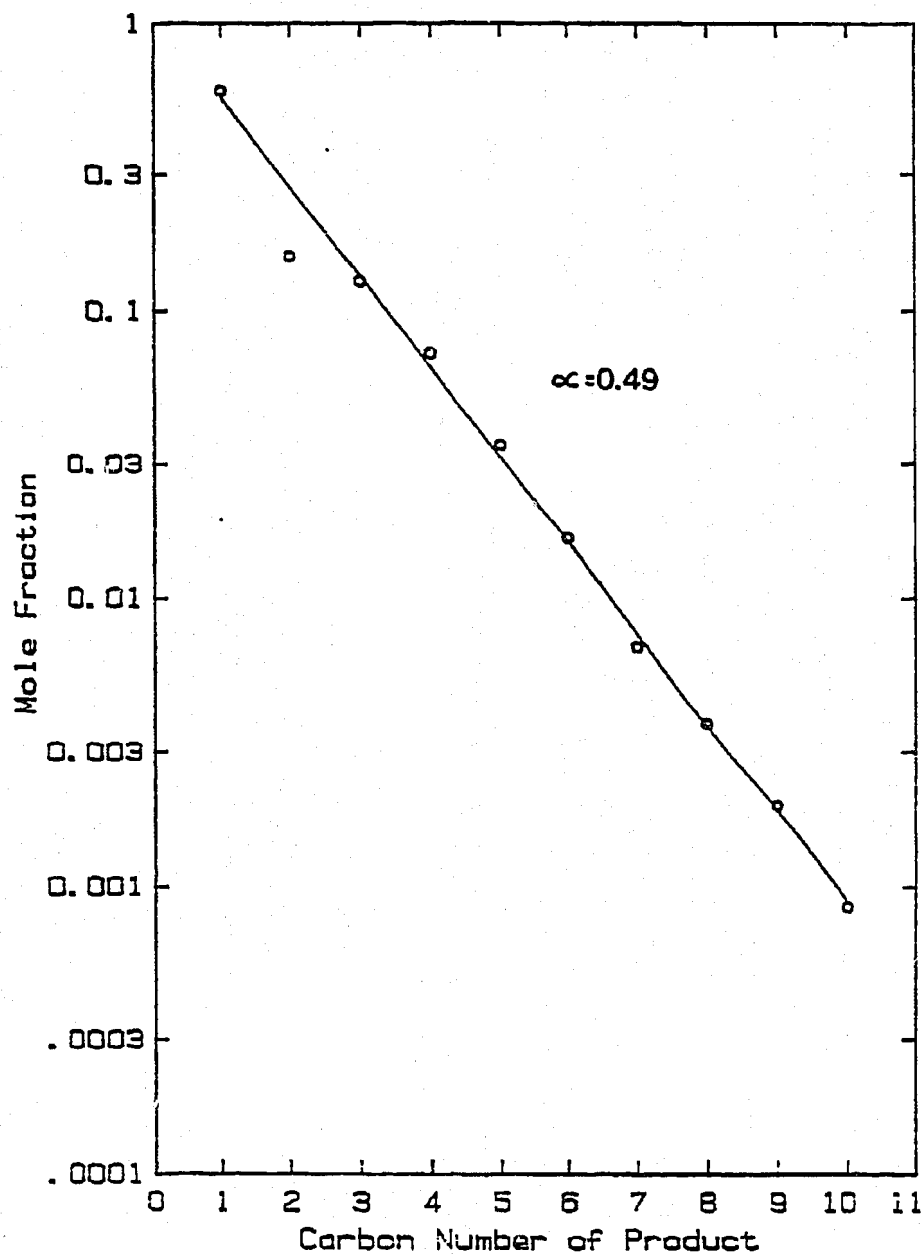


Figure 4.15. A Flory Plot of the Hydrocarbon Product Distribution from Steady-State Fischer-Tropsch Synthesis, Run 8-3 (see Table 4.3 for Experimental Conditions).

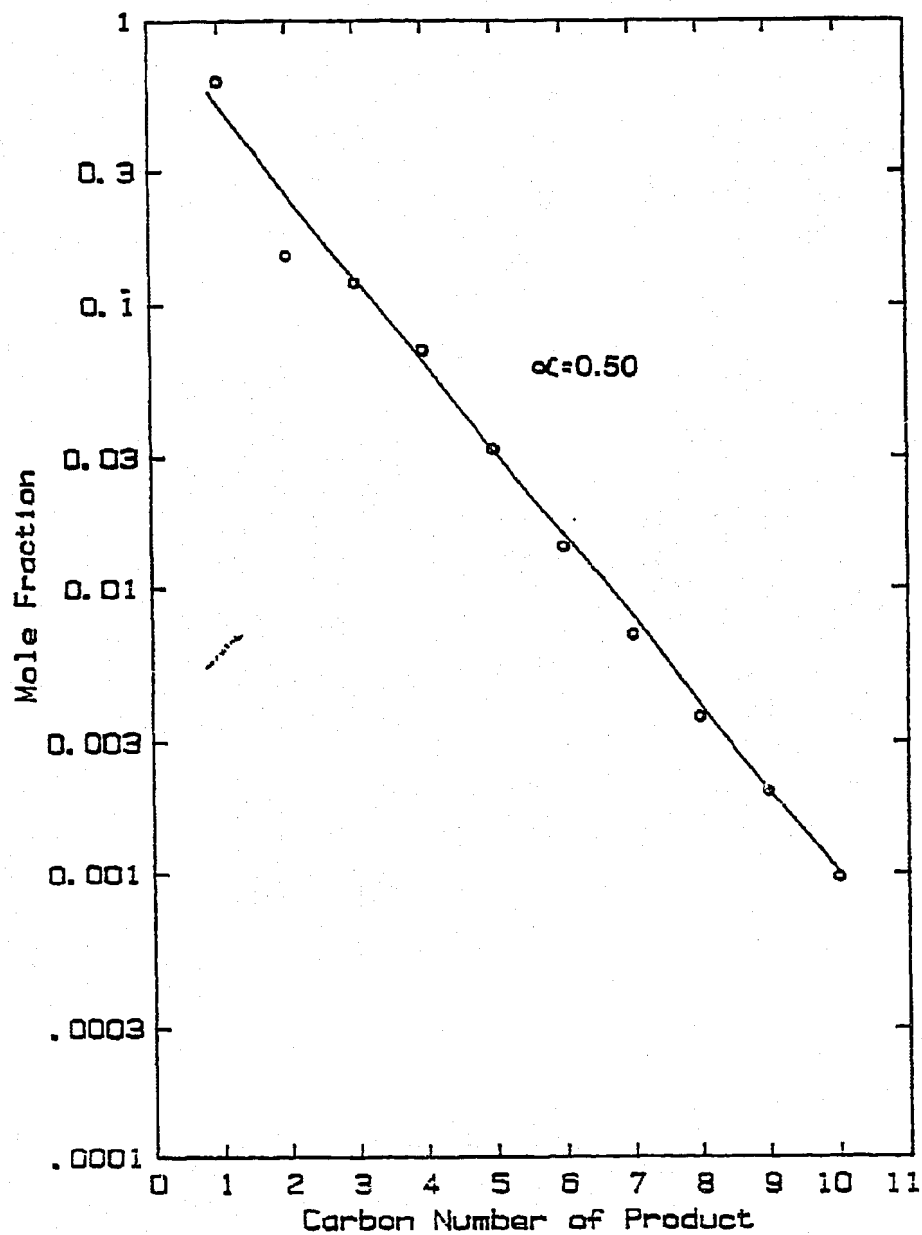


Figure 4.16. A Flory Plot of the Hydrocarbon Product Distribution from Steady-State Fischer-Tropsch Synthesis, Run C-1 (see Table 4.3 for Experimental Conditions).

chain growth (as observed from Figures 4.14 and 4.15) dropped from 0.55 to 0.50. These shifts in hydrocarbon product distribution are the reason why the catalyst was 42% defluidized after 10 hours of synthesis in Run B-3, and why it was not defluidized at all after 2 hours of synthesis in Run C-1.

#### 4.2.3 Steady-State Carbon Deposition Studies

During the defluidization experiments, it was difficult to collect and identify a discrete bugdust fraction. This was caused by condensed liquid products and waxes in the reaction zone, which turned the spent catalyst and bugdust into an agglomerated mass. However, in four of the defluidization experiments, a discrete, free-flowing catalyst fraction and a discrete bugdust fraction could be separated. The bugdust consisted of small particles of low density, which tended to accumulate on the catalyst retention plate, forming a thin black layer. The bugdust layer and the free-flowing catalyst are illustrated schematically in Figure 4.17. The physical separation of these two fractions made it easier to collect the spent catalyst.

##### 4.2.3.1 Trends in Carbon Deposition

Referring to Table 4.3 given in previously Section 4.2, several trends in carbon-deposition rate can be observed. These trends are in agreement with results presented in the literature. Experiments D-1 and C-2 were both performed using a feed gas of 1:1 H<sub>2</sub>/CO ratio. Upon increasing the reaction temperature from 380°C in Run D-1 to 400°C in Run C-2, the weight fraction of bugdust present at the end of the run increased drastically. After 1 hour and 15 minutes of reaction at 380°C,

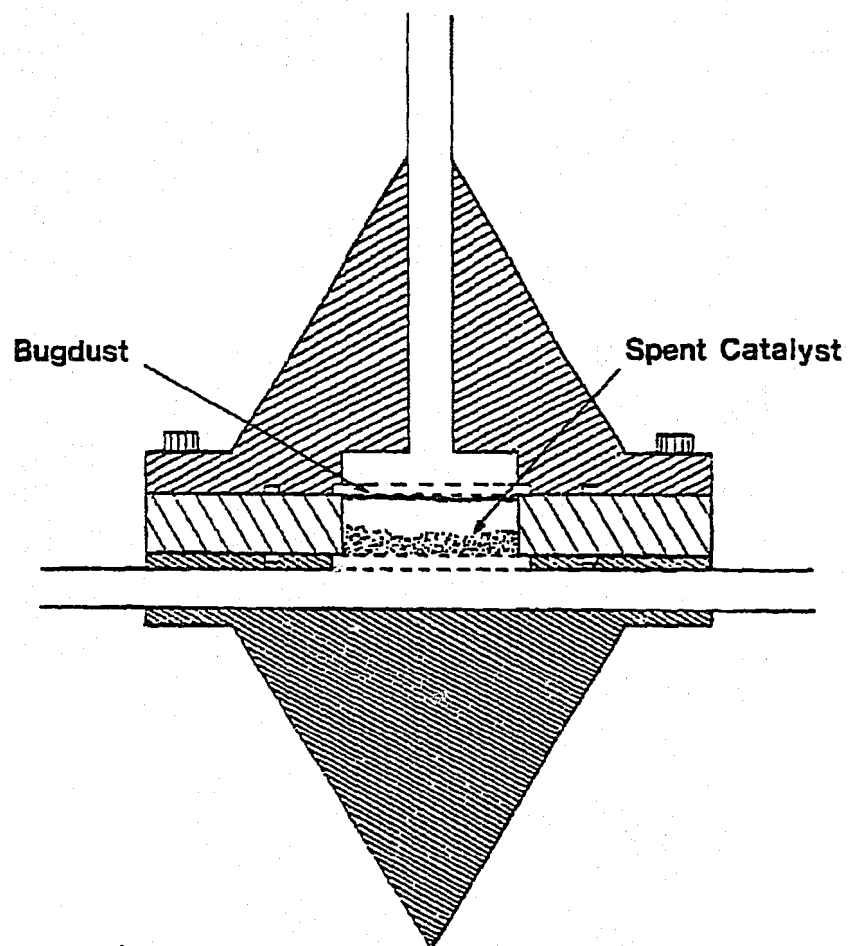


Figure 4.17. An Illustration of the Bugdust Layer and the Free-Flowing Spent Catalyst in the Microreactor After a Steady-State Run.

the reaction zone contained approximately 12 percent bugdust by weight. In contrast, after only 1 hour of reaction at 400°C, the reaction zone contained 100 percent bugdust. Carbon had completely destroyed the physical structure of the fused-iron catalyst. The net weight gain of material in the reaction zone for Run D-1 was 18.1 mg. Run C-2, however, showed a net weight gain of 145.4 mg for the contents of the reaction zone. The gain in weight of the contents of the reaction zone are largely due to accumulation of carbon in the reaction zone.

#### 4.2.3.2 Carbon Deposition at 395°C

As discussed in Section 4.2.1, a synthesis temperature of 395°C, has been identified as sufficient to avoid defluidization of the vibrofluidized fused-iron catalyst. A final group of experiments, Runs F-1 through F-5 as summarized in Table 4.4, involved characterizing the precarburization synthesis period (Runs F-1 and F-2) and then performing baseline, steady-state carbon deposition experiments (Runs F-3, F-4, and F-5). The absolute amounts of free-flowing catalyst and bugdust collected at the end of Runs F-1 to F-5 have been presented previously in Table 4.4.

Table 4.5 lists the elemental and molecular-phase compositions of bugdust and free-flowing spent catalyst fractions for Runs F-1 through F-5. Elemental carbon was determined by coulometric determination of CO<sub>2</sub> after complete oxidation of the sample. Total iron was determined by Atomic Absorption spectroscopy. Both elemental determinations were performed by Galbraith Laboratories, Knoxville, Tenn.

The molecular-phase determinations were performed by Professor P.A. Montano at West Virginia University. Mössbauer spectroscopy was used

TABLE 4.5

Elemental and Molecular Composition of Free-Flowing Spent Catalyst and  
Bugdust Fractions for Baseline Steady-State Fischer-Tropsch  
Synthesis Experiments

Run Number	Spent Fraction	Relative Amount of Each Spent Fraction (wt%)	Elemental Composition (wt%) <sup>a</sup>		Approximate Molecular Composition by Mössbauer Spectroscopy (wt%) <sup>b</sup>		
			Carbon	Iron	$\alpha$ -Fe	$\gamma$ -Fe <sub>5</sub> C <sub>2</sub>	Fe <sub>3</sub> O <sub>4</sub>
F-1	Free-flowing Catalyst	100	7.61	70.47	5	55	40
F-2	Free-flowing Catalyst	100	5.14	72.71	7	56	37
F-3	Free-flowing Catalyst	96.4	7.36	70.64	8	49	43
	Bugdust	3.6	18.82	63.95	- <sup>c</sup>	-	-
F-4	Free-flowing Catalyst	97.2	9.83	69.15	4	54	42
	Bugdust	2.8	29.56	50.60	-	-	-
F-5	Free-flowing Catalyst	92.9	9.13	70.12	8	47	45
	Bugdust	7.1	26.97	56.63	-	-	-

Note: See Table 4.4 for experimental conditions and for absolute amounts of free-flowing catalyst and bugdust fractions collected at the end of each run.

<sup>a</sup>The difference is assumed to be oxygen bound as Fe<sub>3</sub>O<sub>4</sub> and promoters.

<sup>b</sup>Assumes that the (1) particle sizes and (2) Debye-Waller factors are equivalent for all three species.

<sup>c</sup>The small bugdust sample sizes precluded the use of Mössbauer spectroscopy for identification of iron-containing phases.



to identify the iron containing phases in the free-flowing spent catalysts. The approximate quantitative composition of the catalyst was determined by the latter method also.

Figure 4.18 is the Mössbauer spectrum of the spent catalyst from Run F-1. The sites for magnetite ( $\text{Fe}_3\text{O}_4$ ), alpha-iron ( $\alpha\text{-Fe}$ ) and Hägg carbide ( $\chi\text{-Fe}_5\text{C}_2$ ) have been identified in the figure. Figures 4.19 and 4.20 show the Mössbauer spectra of the free-flowing spent catalyst from Runs F-1 through F-3, and F-4 and F-5, respectively. These samples were said to contain similar quantities of the three aforementioned iron-containing phases. If the Mössbauer results were quantitatively accurate, the amount of elemental free carbon in the free-flowing spent catalyst could be determined. Free carbon is not detected by Mössbauer spectroscopy so it must be obtained by difference. This would be done in the following manner.

1. Four phases are attributed to the sample: (1)  $\alpha\text{-Fe}$ ; (2)  $\text{Fe}_3\text{O}_4$ ; (3)  $\chi\text{-Fe}_5\text{C}_2$ ; and (4) free C.
2. The weight percent iron obtained by Mössbauer spectroscopy (molecular determination) is equated to that obtained in the elemental analysis by Atomic Absorption spectroscopy.
3. The weight percent of carbon present as  $\chi\text{-Fe}_5\text{C}_2$  is subtracted from the weight percent of carbon obtained in the elemental analysis.
4. The difference in carbon content can be attributed to elemental free carbon.

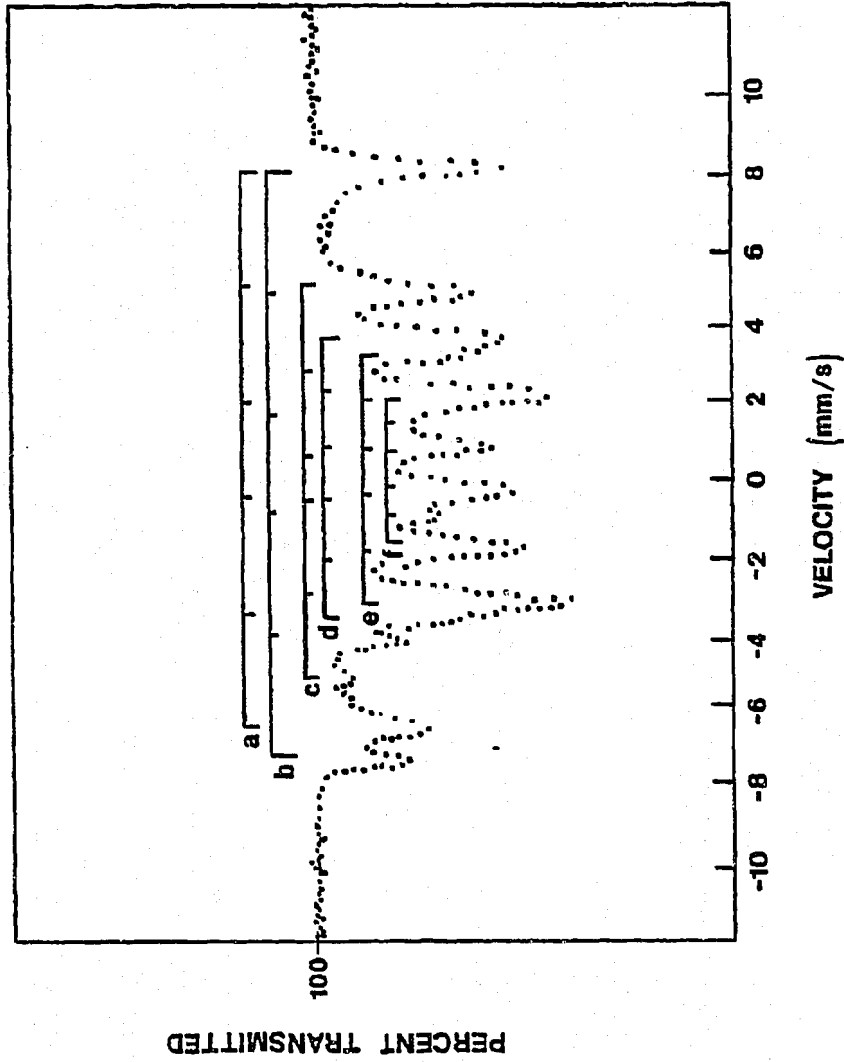


Figure 4.18 A Mössbauer Spectrum of the Free-Flowing Spent Catalyst From Run F-1. Sites include: 1) a and b for  $\alpha$ -Fe; 2) c for  $\text{Fe}_3\text{O}_4$ ; and 3) d, e and f for  $x\text{-Fe}_3\text{C}_2$ .

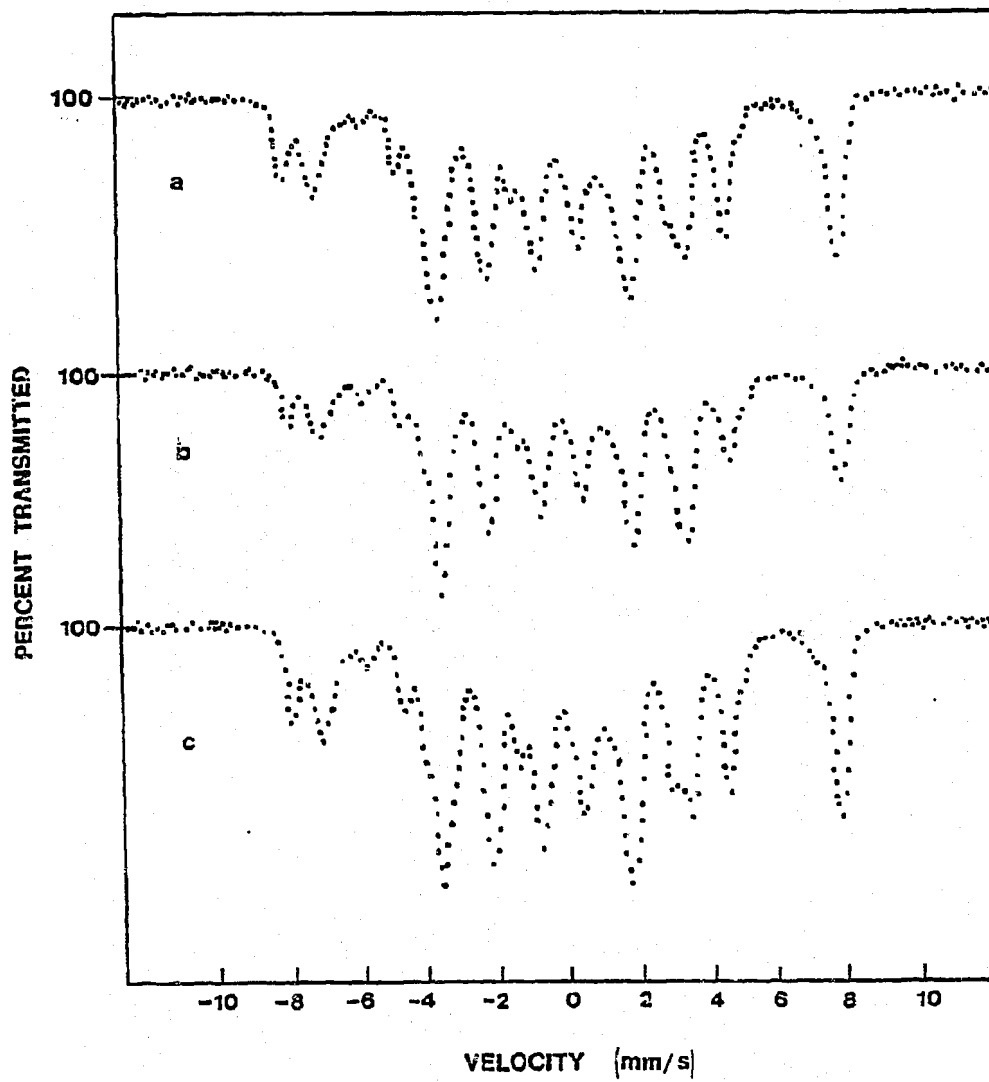


Figure 4.19. The Mössbauer Spectra of Free-Flowing Spent Catalyst From:  
a) Run F-1; b) Run F-2; and c) Run F-3.

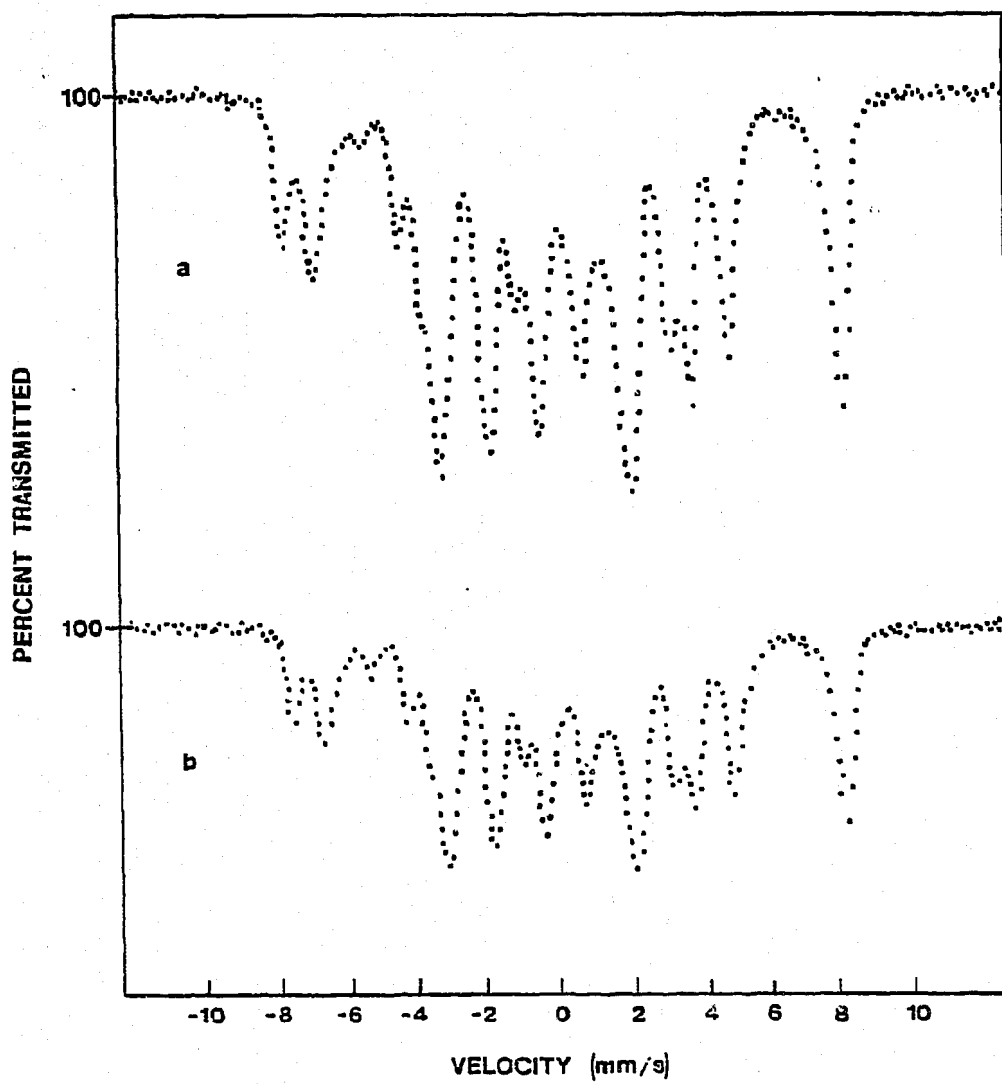


Figure 4.20. The Mössbauer Spectra of Free-Flowing Soent Catalyst From:  
a) Run F-4; and b) Run F-5.

Attempts to obtain elemental free carbon by difference proved futile, presumably because of the approximate nature of the quantitative Mössbauer determinations. One reason for the lack of accuracy may be because the Debye-Waller factors were assumed to be equivalent for all three phases. Cohen (1976) states that the size and parametric dependence of the recoil-free fraction (Debye-Waller factor) is a prime goal of Mössbauer experiments when quantitative analysis is desired. Therefore, the molecular compositions presented in Table 4.5 should be taken as semi-quantitative results.

Table 4.6 is a summary of the total amount of carbon formed, both as carbides and elemental carbon in Runs F-1 through F-5. The time-averaged rate of carbon uptake in the reaction zone has also been calculated for each run. Several useful trends in carbon deposition can be obtained from the results in this table. The time-averaged rate of carbon uptake increases after switching from a gas of  $H_2/CO$  of 4:1 to a gas of  $H_2/CO$  ratio of 2:1 or 1:1. When using a synthesis gas of  $H_2/CO$  ratio of 4:1, the rate of carbon deposition was low and the spent catalyst was gray in color (Runs F-1 and F-2). When a synthesis gas of  $H_2/CO$  ratio of 2:1 or 1:1 was used, carbon deposition was rapid as reflected in the formation of soot and the blackening of the catalyst.

The time-averaged rate of carbon deposition increased nearly six-fold (from 0.385 to 2.478 mg/min) upon switching to a gas of  $H_2/CO$  ratio of 1:1 (Run F-5). In addition, the rate was over five times greater when a synthesis gas of  $H_2/CO$  ratio of 1:1 was used than when one of 2:1 was used. The total weight gain attributed to carbon during

TABLE 4.6  
 A Summary of the Total Amount of Carbon Formed (As Carbides and Elemental Carbon) and the Rate of Carbon Uptake  
 in the Reaction Zone for Runs F-1 through F-5

Run Number	Precarburization Period with a 1/2/CO Gas of 4:1 ratio (min)	Duration of Synthesis (min)	1/2/CO Ratio of Gas Used in Synthesis Period	Total Amount of Carbon in the Reaction Zone After the run (mg)	Carbon as Percent of Total Sample (wt%)	Time Averaged Carbon Uptake During the Precarburization Period (ng/min)	Time Average Carbon Uptake During the Synthesis Period (ng/min)
F-1	110	-	-	70.9	7.61	0.337	-
F-2	120	-	-	46.2	5.14	0.385	-
F-3	120	60	2.08:1	72.9	7.77	0.385 <sup>a</sup>	0.445
F-4	120	120	2.08:1	101.7	10.38	0.385 <sup>a</sup>	0.463
F-5	120	22	1.03:1	100.5	10.40	0.385 <sup>a</sup>	2.468

<sup>a</sup>Assumed carbon uptake rate based on Run F-2.

two hours of synthesis with a gas of  $H_2/CO$  ratio of 2:1 (Run F-4) was the same as that obtained after 22 minutes of synthesis with a gas of  $H_2/CO$  ratio of 1:1 (Run F-5). However, a greater percentage of the carbon was present in the bugdust fraction after Run F-5 than after Run F-4.

#### 4.2.3.3 The Nature of Bugdust

Bugdust is fine, low-density particles consisting of elemental carbon, iron carbides and  $Fe_3O_4$ . It is produced when severe carbon deposition takes place on the surface of the iron catalyst, resulting in eventual breakup of the physical structure of the catalyst.

Figures 4.21, 4.22 and 4.23 are micrographs of a typical bugdust sample taken at magnifications of 100X, 1000X and 10,000X, respectively. Figure 4.21 shows that bugdust consists of irregular-shaped particles, ranging in size from less than  $1\mu$  to more than  $70\mu$ .

Figure 4.22 presents a closer view of individual bugdust particles. The particle inside the bordered area is approximately  $10\mu$  in length. Its surface appears to have a porous structure.

Figure 4.23 is a further enlargement of the particle outlined in Figure 4.22. The surface is a highly porous, coral-like structure. This structure is presumably built up by carbon being deposited on an iron and iron-carbide-bulk structure.

The elemental composition obtained in this study indicates that the bugdust fraction contains 13 to 30 weight percent carbon, 50 to 64 weight percent iron with the remainder present as oxygen and small amounts of promoters.

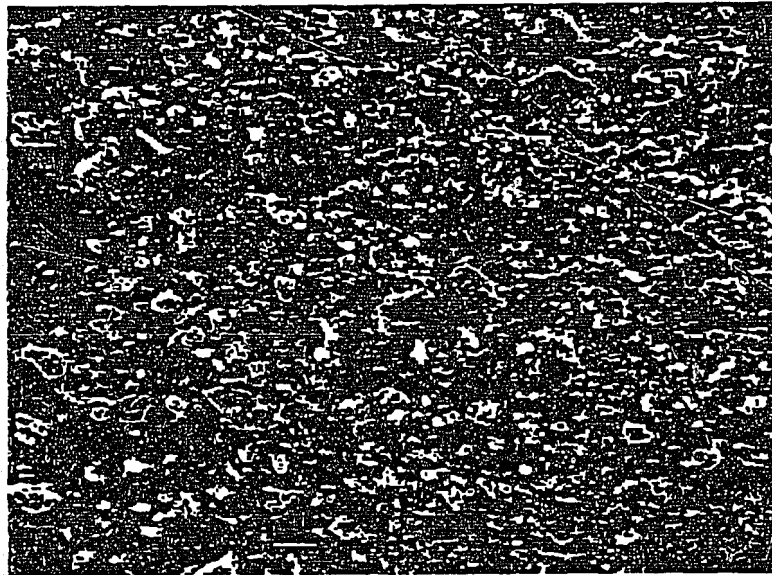


Figure 4.21. An Electron Micrograph of a Typical Bugdust Sample at a Magnification of 100X (1 mm = 10 $\mu$ ).



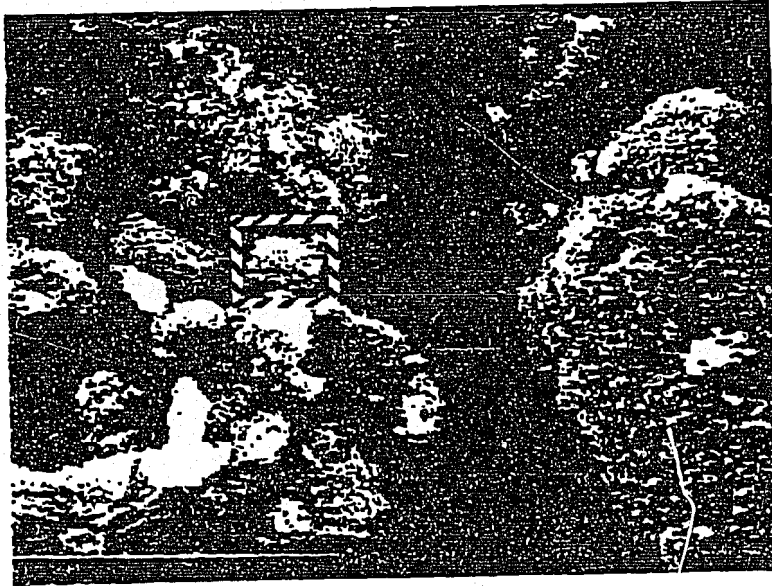


Figure 4.22. An Electron Micrograph of a Typical Bugdust Sample at a Magnification of 1000X (1 mm = 1 $\mu$ ).

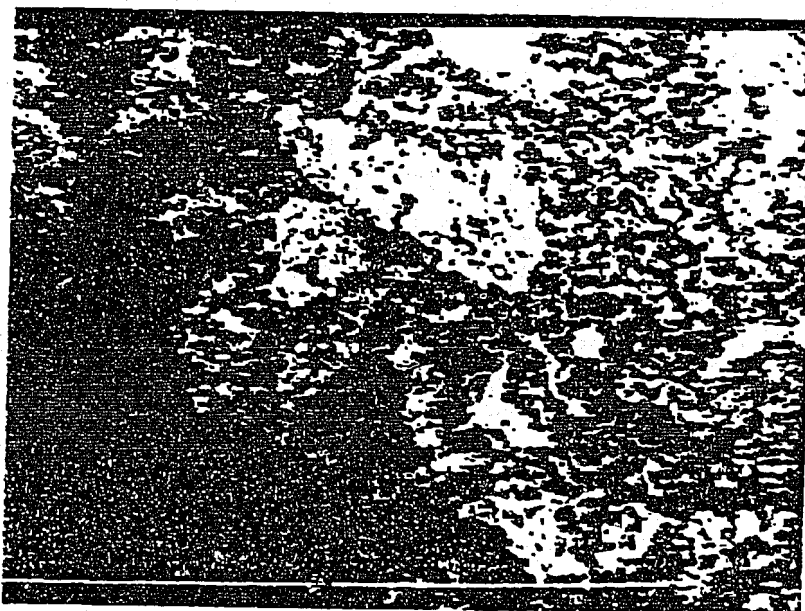


Figure 4.23. An Electron Micrograph of the Surface of the Bugdust Particle Outlined in Figure 4.19 at a Magnification of 10,000X (1 mm = 0.1 $\mu$ ).

## CHAPTER 5

### GAS MIXING AND CATALYST VIBROFLUIDIZATION STUDIES IN A COLD-FLOW VIBROFLUIDIZED-BED MICROREACTOR MODEL

#### 5.1 Apparatus and Procedures

##### 5.1.1 Experimental Apparatus

##### 5.1.1.1 Microreactor Model System

Gas-mixing and differential-pressure measurements were made in a cold-flow model of the unsteady-state vibrofluidized-bed microreactor system. The primary goal of these measurements was to determine the characteristics of the newly-designed, rapidly switching system.

Figure 5.1 is a schematic diagram of the sliding-plug vibrofluidized-bed microreactor system for cold-flow studies. Figure 5.2 is a photograph of the system. Referring to Figure 5.1, argon or helium enters the system through a low-pressure two-stage gas regulator and is stored in a gas reservoir ( $1.0 \times 10^6 \text{ mm}^3$  in volume) made of PVC pipe. Two-way solenoid valves (Precision Dynamics model 2012), controlled through an interface to a Heath H-89 microcomputer, direct which gas is flowing to the microreactor. Flow rates are manually set using double-needle valves (Nupro model 2SGA) located downstream of the solenoid valves. All tubing is 1/4-inch O.D. brass with a 0.035-inch wall thickness. Flexible braided-metal hoses connect the feed and exit lines to the sliding-plug microreactor itself. These hoses allow the microreactor to vibrate, while maintaining a gas-tight seal in the system.

A 0.36-mm diameter wire runs through the 1/4-inch O.D. tubing from each solenoid plunger to the sliding plug in the plenum region of the

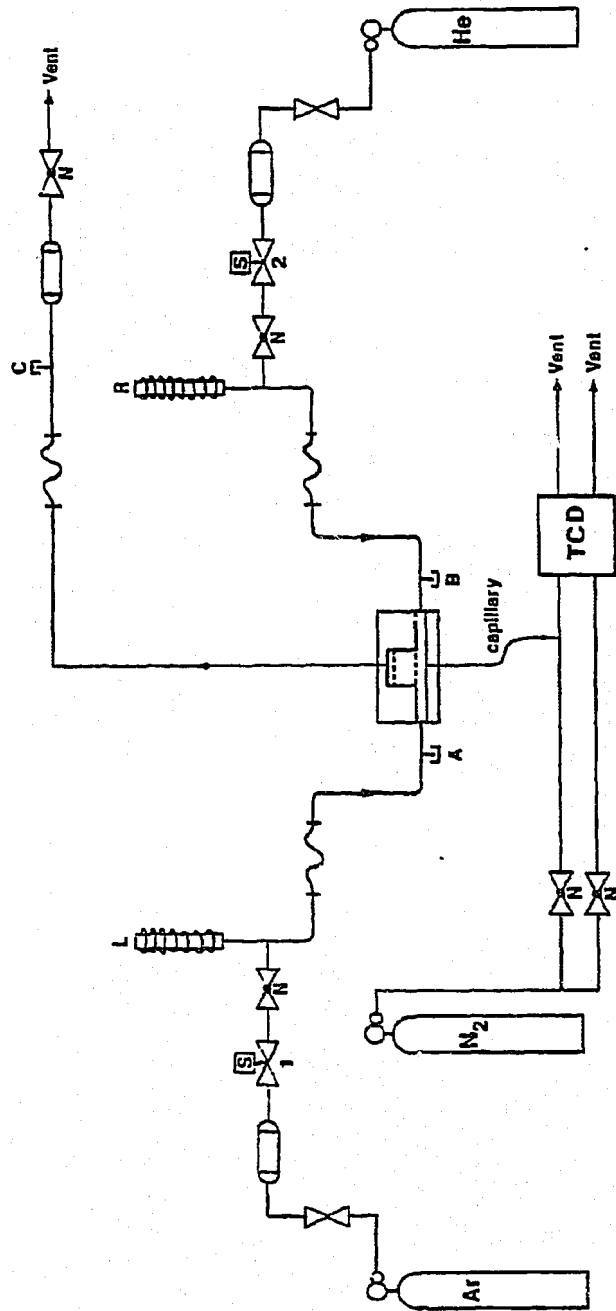


Figure 5.1. A Schematic Diagram of the Sliding-Plug Vibrofluidized-Bed Microreactor System for Cold-Flow Studies (see Figure 4.1b for Equipment Symbols Included in the Figure).

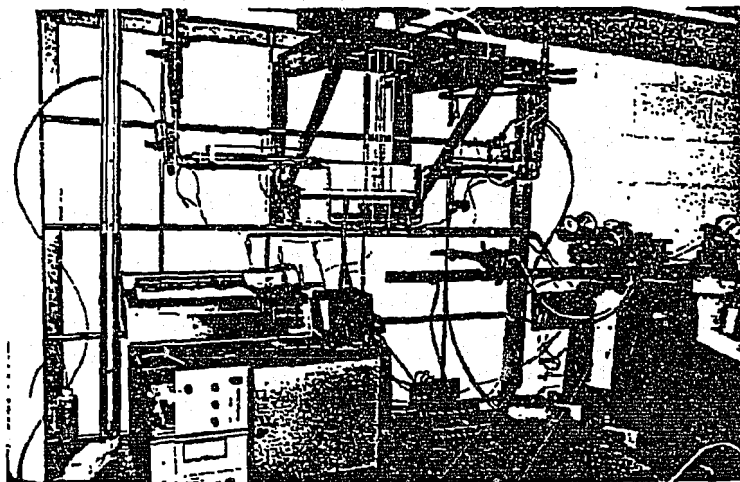


Figure 5.2. A Photograph of the Sliding-Plug Vibro-fluidized-Bed Microreactor System for Cold-Flow Studies.

microreactor. The wire is connected to the plungers and the plug by eyelets. It is threaded through these eyelets and then twisted around itself.

The solenoid design will be examined in Section 5.1.1.3.

Downstream of the microreactor, exit gas is held in a gas reservoir ( $5.0 \times 10^5 \text{ mm}^3$ ) and bled off through a Mupro 4SG needle valve. A pressure tap exists in both feed lines to the microreactor as well as in the exit line. A rapid-response differential-pressure transducer (MKS Instruments model 223AH, 0-100 torr) is used in conjunction with these pressure taps to obtain pressure drop and pressure swing information. The response of the transducer is recorded on a storage oscilloscope (Tektronic T912 10 MHz).

Stainless-steel capillary tubing 1/15-inch O.D. with a 0.028-inch wall thickness allows a small amount of gas to be continuously drawn off from the sliding-plug microreactor. The capillary can be connected to the microreactor in one of three places: (1) the plenum zone; (2) the catalyst zone; or (3) the gas-exit zone. The taps in the microreactor can also be used for differential-pressure measurements. Gas flowing through the capillary from the microreactor bleeds into a stream of pre-purified nitrogen flowing through a 1/8-inch O.D. copper tubing directly to a thermal conducting detector (TCD).

Signal balance is maintained in the TCD through the use of another parallel nitrogen stream set at an equivalent flow rate. The signal from the TCD is recorded using a strip chart recorder (Cole-Parmer model 3386).

The microreactor is vibrated in an identical fashion and by identical equipment as that described in Section 4.1.1.2.

#### 5.1.1.2 Cold-Flow Sliding-Plug Vibrofluidized-Bed Microreactor

Cold-flow model experiments for gas mixing and differential pressure measurements involved the use of the sliding-plug vibrofluidized bed microreactor pictured in Figure 5.3. Cross-sectional schematic diagrams of this microreactor are shown in Figures 5.4 and 5.5. The design and construction features of this microreactor are similar to the steady-state microreactor which was illustrated previously in Figure 4.1 and described in Section 4.1.1.2.

The lexan microreactor consists of three main sections: (1) the base section; (2) the catalyst section; and (3) the gas-exit section. The base section contains a plenum zone in which a sliding brass-plug resides. The plenum consists of a 6.35-mm diameter hole, 76.2 mm in length. At either end of the plenum, a Swagelok straight threaded-fitting connects the feed lines to the plenum.

A groove was machined into the end face of the Swagelok fittings in order to accept a 6.35-mm O.D. rubber O-ring. The O-ring, which has been epoxied to the fitting, serves as a seat for the sliding brass plug. The brass plug is 6.248 mm in diameter and 25.4-mm long. Eyelets extend approximately 3 mm from each end of the plug, so that the connecting wire can be affixed to the plug.

The distributor plate is recessed into a 1.59-mm deep slot in the base section, which is 6.35-mm wide and 25.4 mm in total length. The ends of this slot are rounded.

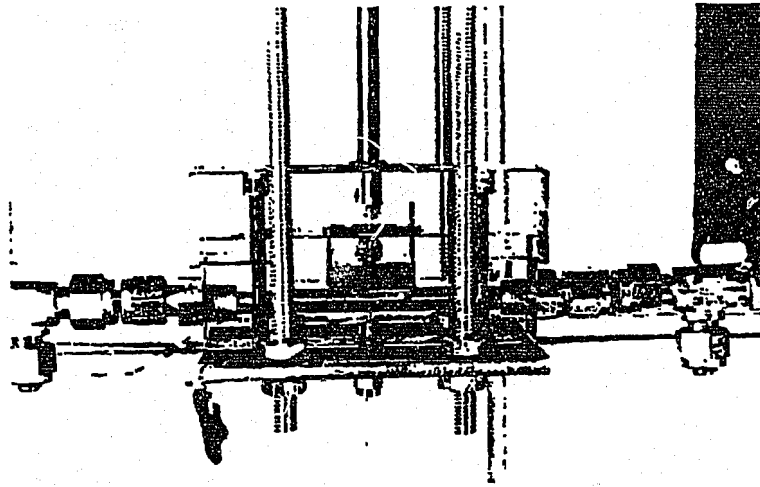


Figure 5.3. A Photograph of the Sliding-Plug Vibrofluidized-Bed Microreactor Model for Cold-Flow Experiments.



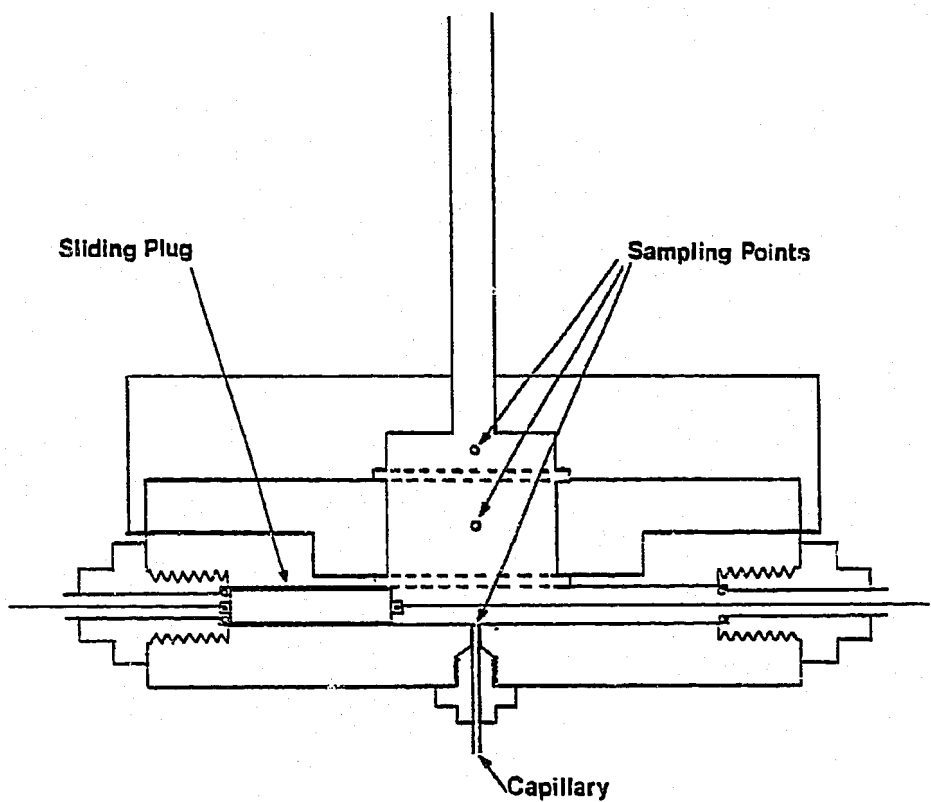


Figure 5.4. A Schematic Cross-Sectional Diagram of the Sliding-Plug Vibrofluidized-Bed Micro-reactor Model (front view).

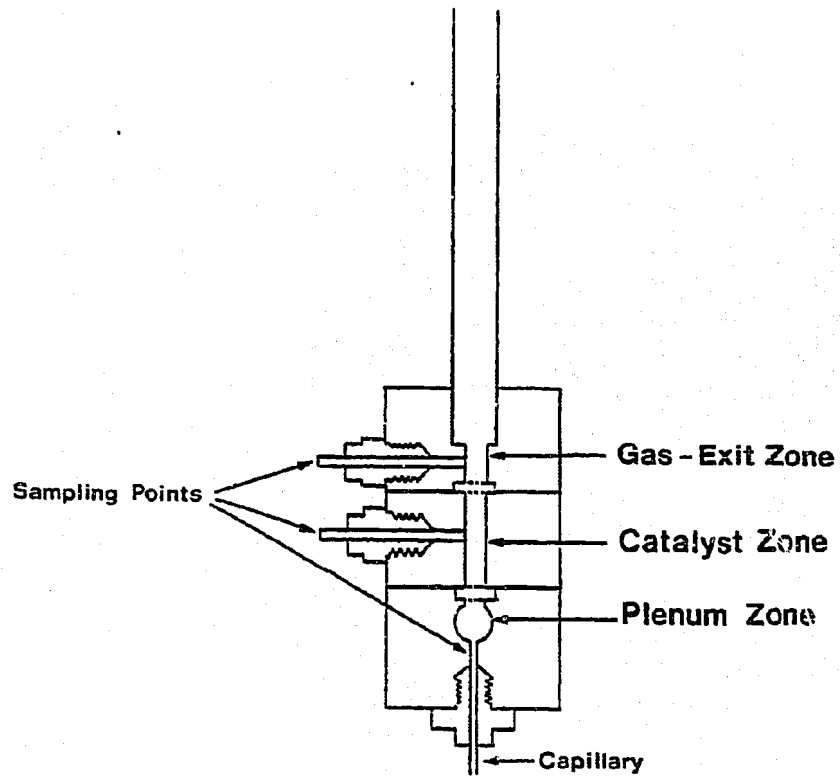


Figure 5.5. A Schematic Cross-Sectional Diagram of the Sliding-Plug Vibrofluidized-Bed Microreactor Model (end view).